Pure Appl. Geophys. 175 (2018), 3485–3509

https://doi.org/10.1007/s00024-018-1871-4

Pure and Applied Geophysics

Analysis of Seasonal Signal in GPS Short-Baseline Time Series

Kaihua Wang,[1,2] Weiping Jiang,[1] Hua Chen,[3,4] Xiangdong An,[1] Xiaohui Zhou,[3] Peng Yuan,[1] and Qusen Chen

Abstract—Proper modeling of seasonal signals and their quantitative analysis are of interest in geoscience applications, which are based on position time series of permanent GPS stations. Seasonal signals in GPS short-baseline (< 2 km) time series, if they exist, are mainly related to site-specific effects, such as thermal expansion of the monument (TEM). However, only part of the seasonal signal can be explained by known factors due to the limited data span, the GPS processing strategy and/or the adoption of an imperfect TEM model. In this paper, to better understand the seasonal signal in GPS short-baseline time series, we adopted and processed six different short-baselines with data span that varies from 2 to 14 years and baseline length that varies from 6 to 1100 m. To avoid seasonal signals that are overwhelmed by noise, each of the station pairs is chosen with significant differences in their height (> 5 m) or type of the monument. For comparison, we also processed an approximately zero baseline with a distance of < 1 m and identical monuments. The daily solutions show that there are apparent annual signals with annual amplitude of ~ 1 mm (maximum amplitude of 1.86 ± 0.17 mm) on almost all of the components, which are consistent with the results from previous studies. Semi-annual signal with a maximum amplitude of 0.97 ± 0.25 mm is also present. The analysis of time-correlated noise indicates that instead of flicker (FL) or random walk (RW) noise, band-pass-filtered (BP) noise is valid for approximately 40% of the baseline components, and another 20% of the components can be best modeled by a combination of the first-order Gauss–Markov (FOGM) process plus white noise (WN). The TEM displacements are then modeled by considering the monument height of the building structure beneath the GPS antenna. The median contributions of TEM to the annual amplitude in the vertical direction are 84% and 46% with and without additional parts of the monument, respectively. Obvious annual signals with amplitude > 0.4 mm in the horizontal direction are observed in five short-baselines, and the amplitudes exceed 1 mm in four of them. These horizontal seasonal signals are likely related to the propagation of daily/sub-daily TEM displacement or other signals related to the site environment. Mismodeling of the tropospheric delay may also introduce spurious seasonal signals with annual amplitudes of ~ 5 and ~ 2 mm, respectively, for two short-baselines with elevation differences greater than 100 m. The results suggest that the monument height of the additional part of a typical GPS station should be considered when estimating the TEM displacement and that the tropospheric delay should be modeled cautiously, especially with station pairs with apparent elevation differences. The scheme adopted in this paper is expected to explicate more seasonal signals in GPS coordinate time series, particularly in the vertical direction.

Key words: Monument thermal expansion, seasonal signal, GPS short-baseline, noise characteristic.

1. Introduction

There are apparent seasonal signals in position time series of GPS permanent stations (Blewitt et al. 2001). The velocities of GPS stations and their uncertainties, which are widely used in monitoring of global change and geophysical applications, can be precisely estimated if the seasonal signals are better understood and modeled (Dong et al. 2002; Santamaría-Gómez et al. 2011; Altamimi et al. 2016). The coexistence of various error sources of seasonal signals and their interactions make the conditions more complex. Ideally, seasonal signals should not be in GPS position time series for short-baselines because most common mode errors and the influence of large-scale geophysical effects are expected to be reduced to negligible levels by double-differencing. However, they are still observed in GPS short-baseline time series with maximum annual amplitudes exceeding 2 mm (King and Williams 2009; Hill et al. 2009), which cannot be tolerated in millimeter-precision deformation monitoring of bridges and dams based

Electronic supplementary material The online version of this article (https://doi.org/10.1007/s00024-018-1871-4) contains supplementary material, which is available to authorized users.

[1] GNSS Center, Wuhan University, Wuhan, People's Republic of China. E-mail: wkh651010@126.com; wpjiang@whu.edu.cn; xdan_619@163.com; yuanpeng@whu.edu.cn

[2] Collaborative Innovation Center of Geospatial Technology, Wuhan University, Wuhan, People's Republic of China.

[3] School of Geodesy and Geomatics, Wuhan University, Wuhan, People's Republic of China. E-mail: hchen@sgg.whu.edu.cn; xhzhou@sgg.whu.edu.cn; chenqs@whu.edu.cn

[4] Key Laboratory of Geospace Environment and Geodesy, Ministry of Education, Wuhan University, Wuhan, People's Republic of China.

on GPS short-baselines (Jiang et al. 2012). Proper modeling and quantitative analysis of these seasonal oscillations should be adopted to better understand the geophysical mechanisms.

The origins of the seasonal signal in position time series for a typical permanent GPS station include two parts. One is the artificial part, such as GPS technical errors during data processing, including the draconitic year cycle (Ray et al. 2007) and high-order ionospheric delay errors (Deng et al. 2016). The other is real site motion induced by geophysical processes, such as solid and ocean tides, surface loadings, thermal expansion, and other local effects (Blewitt et al. 2001; Dong et al. 2002; Tregoning and van Dam 2005; Yan et al. 2009). Errors may also be introduced when aligning the GPS network to the reference frame (Collilieux et al. 2010). The propagation of unmodeled or mismodeled sub-daily signals may also contribute to spurious long-period signals (Penna and Stewart 2003; Penna et al. 2007). For position time series of GPS short-baselines, most common mode errors related to the GPS itself have been eliminated or greatly degraded. Furthermore, the effects of large-scale geophysical phenomena (e.g., ocean tides, surface loadings) on station pairs with short distances are nearly equivalent, so they will also be eliminated. Thus, the remaining potential contributors to seasonal signal in GPS short-baseline position time series include TEM, local effects and other site-specific errors, such as multipath and soil moisture.

As an elastic response to temperature variations, the amplitude of the TEM is mainly determined by the monument height and the amplitude of the temperature variation (Dong et al. 2002; Yan et al. 2009). Different material types and structures of the GPS monuments make the circumstance more complicated (Haas et al. 2013; Munekane 2013). Recent studies have applied GPS short-baselines to study site-specific effects, and have reached a consensus that TEM may be one of the potential contributors to the seasonal signal (King and Williams 2009; Hill et al. 2009; Santamaría-Gómez 2013). The annual amplitudes for the adopted GPS short-baselines generally exceed 0.5 mm on both the vertical and horizontal components, but only part of the annual signal can be explained by TEM based on a simple linear expansion model (King and Williams 2009). The results of a GPS short-baseline network of braced monuments (Hill et al. 2009) indicates that the seasonal cycle, which is consistent with local temperature data, may be related to thermal expansion of the bedrock (TEB). Similar seasonal signals are also observed by Santamaría-Gómez (2013), which may be derived by thermally induced displacement of the edge of the building beneath the monument caused by direct solar heating. Other independent observations derived from thermal tilt (Munekane 2013) and total station (Lehner 2011; Haas et al. 2013) data have also been applied to verify the apparent impact of TEM, with annual amplitude up to 1 mm and sub-daily variation up to 3 mm on the horizontal component.

In addition to TEM and TEB, the tropospheric delay error induced by imperfect data processing strategy may also introduce aliased seasonal signal in GPS short-baseline time series (Munekane and Boehm 2010), especially for baselines with large height differences (Schön 2006). Although site-specific errors, such as multipath, can introduce sub-daily signals at $\sim$ K1 and $\sim$ K2 bands in GPS coordinate time series (King and Williams 2009; King and Watson 2010), multipath is likely unable to explain annual signals of > 0.2 mm that are observed in GPS short-baseline position time series. The propagation of these high-frequency signals to spurious annual or semi-annual signals (Penna et al. 2007; King et al. 2008) makes the explanation of the seasonal signal more complicated and requires further investigation.

To obtain authentic and reliable seasonal characteristics, the optimal noise model (ONM) should be determined in advance to best describe the stochastic process in GPS short-baseline time series. Although different noise models have limited impacts on velocity and seasonal amplitude estimates, they can enlarge the uncertainties, especially for time series with short time spans (Williams 2003; Santamaría-Gómez et al. 2011; Langbein 2012). Previous studies have suggested the ONM for most global IGS stations can be described by a combination of FL and WN (Williams et al. 2004; Langbein 2008). Some stations can be modeled by RW, which characterizes the random motion of the monument itself, and observations from electronic distance measurements indicate that almost 40% of baselines can be best

modeled by BP noise (Langbein 2004). The ONM for GPS short-baseline time series still requires further and comprehensive study because the monuments vary between sites.

Despite the comprehensive analysis of monument stability by King and Williams (2009), there are still several problems with the origins of seasonal signal in GPS short-baseline time series. For example, only part of the seasonal signal observed in the vertical direction can be explained by TEM. This may be caused by several reasons: (1) deviations in the estimations of the observed amplitude and uncertainties due to the limited time span and determination of the noise model; (2) deviations in the estimations of the TEM amplitude due to an inaccurate model, which ignores thermal expansion of the concrete building beneath the monument or the underground part of the monument itself; and (3) the thermally induced displacements of the short-baselines may be overwhelmed by other signals or errors, which may bias the result. In addition, the apparent horizontal annual signals observed by King and Williams (2009) and Hill et al. (2009) can rarely be explained by known causes.

To clarify these questions and better understand the seasonal signals exhibited in GPS position time series, we processed GPS observations of 6 short-baselines with distances less than 1.1 km and one approximately 'zero baseline' for comparison. The time spans vary from 2 to 14 years, which is much longer than those processed by King and Williams (2009). In contrast, station pairs with identical monuments are chosen for the 'zero baseline'. Detailed information about the short-baselines and GPS processing strategy are described in Sect. 2. The results of seasonal terms and noise characteristics of the GPS short-baseline position time series are presented in Sect. 3. In Sect. 4, the potential origins of the seasonal signals in position time series for the adopted GPS short-baselines are discussed in detail.

2. *Dataset and GPS Processing*

2.1. *Selection of Short-Baselines*

To ensure that the thermally induced monument motion is isolated from the noise in GPS position time series, the signal should be enlarged by choosing station pairs with large differences in height and the type of the monument. The station pairs of the short-baselines adopted in this paper followed the criteria below: (1) baseline length $\leq$ 1.1 km and elevation difference $\leq$ 120 m; (2) overlapping observations available $\geq$ 2 years after epoch 2000.0; (3) monuments with height difference $\geq$ 5 m or with obvious differences either in type or structure; and (4) stable IGS stations with less offsets induced by equipment change. Thus, six IGS station pairs with baseline lengths from 6 to 1100 m and an approximately 'zero baseline' with identical monuments were adopted. Table 1 lists a summary of the selected baselines.

GPS observations were provided by SOPAC, and details of the monuments were obtained from either the item 'height of monument' or personal communication with the responsible organization listed in the station log files (ftp://garner.ucsd.edu/archive/garner/docs/station_logs). Stations TCMS and TNML were all settled on roof of a $\sim$ 8-m-high building (see auxiliary material 1). The monument of TCMS was composed of a steel mast with a height of 1.87 m, while the monument of TNML was a steel truss with a height of 2.09 m. The monument of station ZIMJ was on the roof of a one-story building, whereas the antenna of station ZIMM was located on top of a steel truss with a height of $\sim$ 9.2 m and an underground length of $\sim$ 1.5 m (see auxiliary material 2). Station JOZE was affixed on a 1-m-high concrete pillar with a foundation depth of 2.5 m, and JOZ2 was located on the roof of a $\sim$ 16.5-m-high building (see auxiliary material 3). Similarly, HERT was mounted on a small brick monument on the corner of a brick water tower $\sim$ 5.5 m above the ground, and the height of the steel truss beneath the antenna of station HERS was $\sim$ 12 m (see auxiliary material 4). Stations OBE2 and OBET were operated for many years and were replaced by a new station (OBE3). The limited available information suggested that these two stations were located on the roofs of buildings that were 4.5 and 10 m high, respectively. MCM4 and CRAR were located at the McMurdo site in Antarctica (see auxiliary material 5). The former station was directly anchored to the bedrock, whereas the latter was attached to a mount on top of a steel

Table 1

Station pairs, length, height difference, common dataset, and height, type, and foundation of the monuments of each short-baseline

Station	Length (m)	Diff. E[b].(m)	Lon. (°)	Lat. (°)	Monument			Common dataset
					Base	Height[c]	Type[d]	
Experimental group								
TCMS[a]	6	0	121.0	24.8	Roof	1.9	SM	2005.001–2012.270
TNML					Roof	2.1	SM	
ZIMJ[a]	14	5.1	7.5	46.9	Roof	4.0	CP	2003.001–2010.295
ZIMM					Bedrock	10.7	SM	
JOZ2[a]	83	11.1	21.0	52.1	Roof	3.5	CP	2002.295–2016.239
JOZE					Bedrock	16.5	CP	
HERT[a]	136	6.9	0.3	50.9	Roof	5.5	CP	2003.078–2016.239
HERS					Bedrock	12.0	SM	
OBE2[a]	268	3.5	11.3	48.1	Roof	4.5	CP	2003.160–2005.129
OBET					Roof	10.0	CP	
MCM4[a]	1100	117.9	166.7	− 77.8	Bedrock	0.1	CP	2002.169–2016.239
CRAR					Roof	7.5	SM	
Control group								
REYK[a]	1	0	338.0	64.1	Roof	13.5	CP	2000.001–2007.261
REYZ					Roof	13.5	CP	

[a]The reference station of the baseline

[b]Diff. *E*. is the difference in station elevation

[c]Monument height is the distance from the top of the monument to the ground in meters

[d]Type of the monument includes concrete pillar (CP) and steel mast (SM)

truss ($\sim$ 2.5 m high), which was affixed to a $\sim$ 5-m-high platform. The two stations of the control group were all settled on the roof of the same building approximately 13.5 m above the ground (see auxiliary material 6).

2.2. GPS Data Processing Strategy

GPS short-baselines were processed with the GAMIT software package (Herring et al. 2010). The observations were differenced twice for each station pair to eliminate the influence of common technical errors and large-scale geophysical processes. The sampling interval was 30 s, and the daily solution was derived by the Kalman-filter from each 24 h session. L1_ONLY was adopted to prevent noisier solutions from the LC observations except for IGS station pairs MCM4 and CRAR, which had a height difference greater than 100 m. LC_AUTCLN was adopted for this baseline, and the zenith tropospheric delay was estimated every 2 h. Otherwise, the strategy for each baseline was identical. The final precise satellite orbits were provided by IGS. The elevation cutoff was chosen by 15°. The L1 and L2 observations were used to estimate the ambiguities with success rates $> 99\%$.

The stations shown in Table 1 above for each station pair were set as the reference stations, and the relative positions were estimated as the baseline solutions on all four components: North, East, Up and Length (N, E, U, and L, respectively). Before analyzing the GPS short-baseline time series, the following three preprocessing steps were adopted: (1) removing outliers with absolute tolerances of 0.01 and 0.015 m from the median from the time series for the horizontal and vertical components respectively, or formal errors greater than 0.1 m for any of the components; (2) removing accidental errors beyond a threshold of 4δ (the root mean square error δ was replaced by the standard deviation); and (3) applying a moving average over 15 days. Sharp steps may be present in some of the baselines due to equipment changes or other unavoidable events, so we examined the events recorded in the site logs carefully to minimize the impact of jumps on estimates of the seasonal terms and noise characteristics.

3. Results

3.1. GPS Short-Baseline Time Series

Figures 1, 2, 3, 4, 5, 6, and 7 show residual time series of the GPS short-baselines TCMS-TNML (TCTN for short), ZIMJ-ZIMM (ZIZI), JOZ2-JOZE (JOJO), HERT-HERS (HEHE), OBE2-OBET (OBOB), MCM4-CRAR (MCCR) and REYK-REYZ (RERE), respectively. Generally, apparent periodical signals are present on most of the components. For baseline TCTN with length of 6 m, position time series on all the components are much quieter than those of other baselines, which indicates the good quality of the baseline solutions. The solutions for ZIZI are slightly more scattered than other baselines on both the *N* and *E* components, especially from January 2004 to July 2006. Similar scattered characteristics occur on JOJO from January 2005 to July 2007 and on HEHE from October 2013 to February 2015. On the U component of baseline MCCR, the formal errors before October 2005 are much larger than in any other periods. In contrast, the time series of the 'zero-baseline' with identical monuments are much quieter than other baselines. In addition, there are abnormal annual peaks on the N and U components of ZIZI and JOJO from December to February of the following year. The peaks only occur during the winter and last for several weeks, and they appear to be annual signals rather than noise. The variations reach 8 mm on the vertical component of JOJO, which indicates that the elevation difference of the station pairs increases to $\sim$ 1 cm compared with other periods of the year.

To estimate the seasonal terms in the position time series, a generalized site motion model is adopted with a linear trend, an offset, annual and semi-annual amplitudes and phases, and a stochastic process ε considered.

$$y = a \cdot t + b + A_1 \cos(2\pi \cdot t + \varphi_1) + A_2 \cos(4\pi \cdot t + \varphi_2) + \varepsilon, \quad (1)$$

where y is the baseline solution of each component, a and b are the linear trend and offset of the GPS time series, respectively, and A and φ are the amplitude and phase of each harmonic, respectively. Two harmonics, which refer to the annual and semi-annual cycles, are chosen and will be discussed in Sect. 3.3. The 'optimal' stochastic process models or different combinations are chosen using the maximum likelihood estimation (MLE) method, which will be discussed in Sect. 3.2. The linear trend and seasonal patterns are then estimated simultaneously under the assumption of the selected noise model, including the corresponding amplitude and phase estimations.

Overall, the linear trend and offset of the short-baselines are estimated before the residual time series are obtained, and they are listed in Table 2. Most of the baselines have linear trends within $\pm$ 0.4 mm/year except for baseline MCCR, whose trend is $-$ 0.74 mm/year on the *N* component. Because most of the common signals and errors have been eliminated to negligible levels, the obvious trend seems to be results of monument wander or other site-specific processes (King and Williams 2009; Hill et al. 2009). Baseline RERE also has a trend of $>$ 0.4 mm/year on the vertical component. For the residuals, the average RMSs are 0.7, 1.0, 1.3 and 0.9 mm on the *N*, *E*, *U* and *L* components, respectively, which indicates the reliability of the solutions. The solutions for baseline JOJO have larger RMSs than those of other baselines with scale factors of 2–3, especially for the E component.

3.2. Noise Characteristics

In this section, a limited analysis of the noise characteristics of the GPS position time series is performed. The CATS software package (Williams 2008) is used to determine the ONM to best characterize the stochastic signal of the residuals. In addition to the FL and RW models, the stochastic process of GPS short-baseline time series can be described by other noise models, such as power-law (PL), first-order Gauss-Markov (FOGM), and BP or their combinations (Langbein 2004, 2008; King and Williams 2009; Hill et al. 2009). For example, FL noise is likely related to GPS systematic errors, RW noise is probably a result of monument motion (Langbein 2008), and BP noise is useful for modeling noise sources with an annual periodicity in GPS position time series (Langbein 2004).

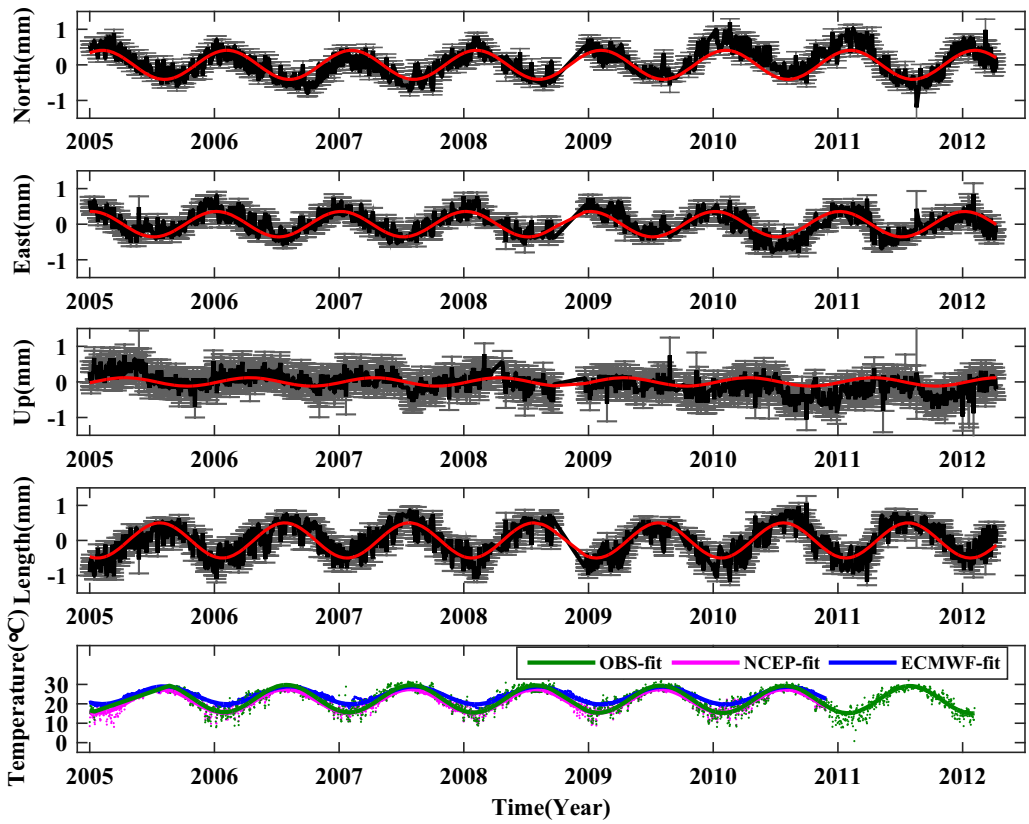

Figure 1
GPS position time series of baseline TCTN (length: 6 m) and the temperature data. The black and gray lines are the solutions and former errors, respectively, for each component, and the red line is the annual cycle fitted with a model consisting of an offset, a linear trend and annual terms. The green, purple and blue dots are the observed local temperature and land surface temperature data from the NCEP and ECMWF numerical models, respectively, and the corresponding lines are the fitting results from applying only the annual term for the dataset in the bottom panel. The scale is identical to other baselines in Figs. 2, 3, 4, 5, 6, and 7

Although adopting different noise models has a limited influence on estimations of the velocity and seasonal amplitude, it can increase the uncertainty of the velocity and may bias the understanding of the stochastic process in GPS position time series (Williams 2003; King and Williams 2009; Langbein 2012). Based on previous studies, seven candidate noise models or combinations of noise models are selected to describe the stochastic process of the GPS baseline time series in this paper: FL, RW, PL, FLRW (the combination of FL and RW), BPPL (the combination of BP and PL), BPRW (the combination of BP and RW), and FOGMRW (the combination of FOGM and RW). These noise models all contain WN. The criterion and method to select the ONM is derived from Langbein (2004) based on the MLE method with the CATS software. First, the initial model is selected with a larger MLE value between the RW and FL. Then, the MLE values of PL and FLRW are estimated and compared to that of the initial model minus a threshold of 2.6, and the noise model with the larger MLE value is marked; otherwise, the initial model is marked. Similarly, the MLE values of the BPPL, BPRW and FOGMRW models are compared to that of the marked model successively as in the previous step with thresholds of 2.6, 2.6 and 5.2 respectively. Eventually, the ONM is selected.

Table 3 shows the distribution of the ONM and the estimated noise parameters for each component of the baselines. The results show that the ONM of each component of the short-baseline varies. In addition to FL, BPPL and FOGMRW are also present, such as on all components of baselines ZIZI and OBOB, and on the N and U components of baseline HEHE.

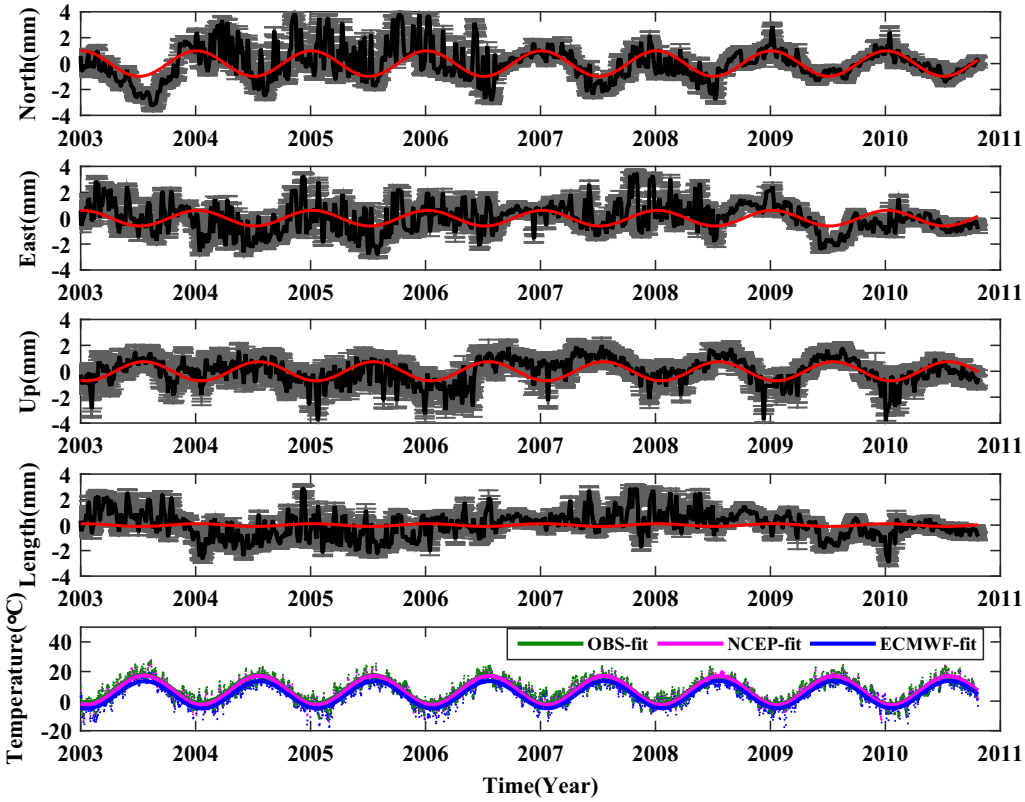

Figure 2
GPS position time series of baseline ZIZI (length: 14 m) and the temperature data

Generally, for the baseline in the control group, ~ 78% (14/18) of the components can be best modeled by either BP or RW.

For the BPPL model, seven extra parameters must be estimated besides the MLE value: the center frequency, width, pole numbers of the band-pass filter noise, spectral index of PL, and amplitude of BP, PL, and WN. Similarly, for the BPRW model, the spectral index is fixed at − 2, and the amplitude of RW is estimated. For the FOGMRW model, an additional beta is estimated for the FOGM model along with the amplitude of each noise. The ONM for each baseline component appears to be disordered, especially for the baseline in the control group. FL and PL dominate the components of the JOJO and MCCR baselines, whereas BP and RW are in the majority of the ZIZI and OBOB baselines. FOGM is only present in the ZIZI and HEHE baselines. It is worth mentioning that RW noise model best describe the stochastic processes of all three components of the RERE baseline, whose monuments are identical. This may indicate that although almost all of the monument motion is differenced in the GPS baseline time series, the noise still exhibits the characteristics of random walk, which are related to the monument itself.

3.3. Seasonal Signals

Before the seasonal terms are estimated, the power spectral densities for the components of the short-baselines in the experimental group and the control group are estimated and are shown in Figs. 8 and 9, respectively. For baselines in the experimental group with significant differences in the monument type or height, there are obvious periodic signals around the annual cycle in the position time series in both the horizontal and the vertical directions. The semi-annual signal is also present on some of the

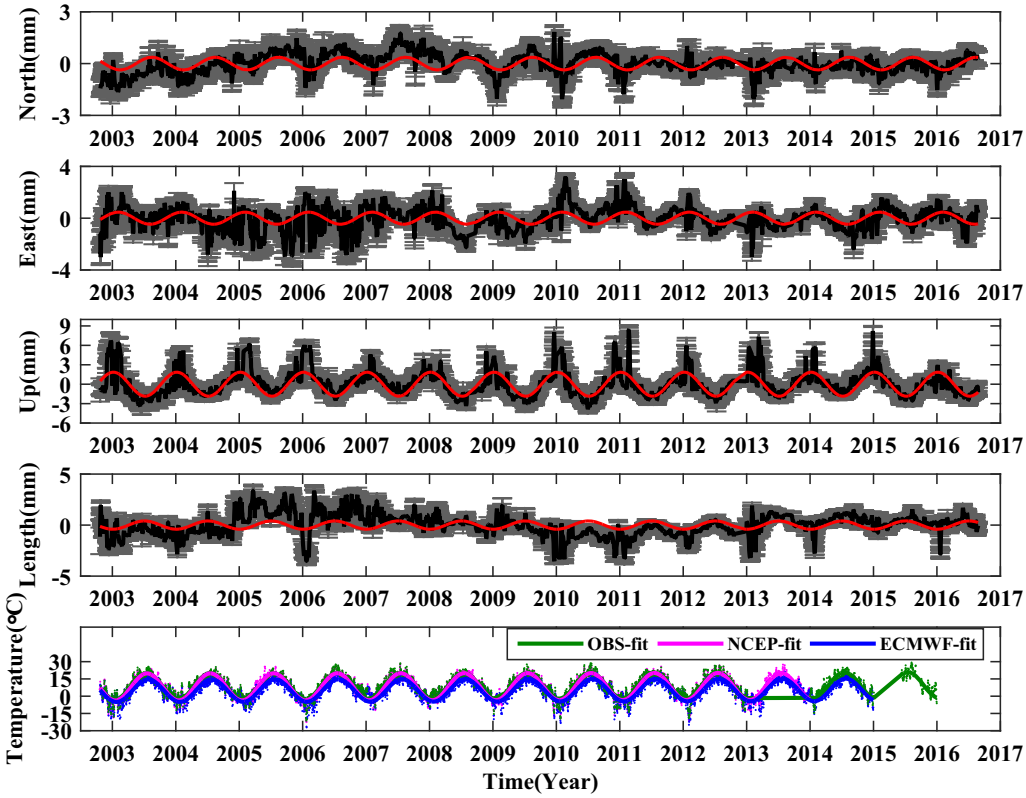

Figure 3
GPS position time series of baseline JOJO (length: 83 m) and the temperature data

components, such as the *N* and *E* components of ZIZI and the *E* and *U* components of HEHE and MCCR. In the control group with identical monuments, there are no significant seasonal peaks on all the three components.

The annual and semi-annual amplitudes and phases are estimated by Eq. (1), and the results are listed in Table 4. The median annual amplitudes of the selected GPS short-baselines are 0.64 ± 0.13 and 0.12 ± 0.14 mm for the test and control groups, respectively, with a maximum amplitude of 1.86 ± 0.17 mm on the U component of baseline JOJO. Compared with the annual amplitude for the single station provided by SOPAC (the annual amplitudes of IGS stations JOZE and JOZ2 are 4.53 ± 0.10 and 5.67 ± 0.20 mm, respectively), the seasonal signal must be handled carefully, especially in GPS short-baseline solutions in which the common mode errors and geophysical signals have been reduced to negligible levels. Among the six baselines in the experimental group, 38% (9/24) of the components have annual amplitude greater than 0.9 mm. In contrast, the annual amplitude for each component of baseline RERE is no more than 0.3 mm. Interestingly, although the difference in the monument heights of stations TCMS and TNML is less than 20 cm, the annual amplitude of baseline TCTN is 0.42 ± 0.03 mm for the *N* component, which is 3 times larger than that of baseline RERE, which has identical monuments. For the same baseline, the semi-annual amplitude is much smaller than the annual amplitude by an average scale factor of ∼ 0.4. In addition, the amplitudes of the annual and semi-annual cycles in the vertical direction are not always greater than those in the horizontal direction, which is inconsistent with the GPS coordinate time series for single stations. For example, the maximum annual amplitude occurs on the *N* component of the ZIZI baseline, whereas the annual amplitudes of baselines HEHE and OBOB are almost

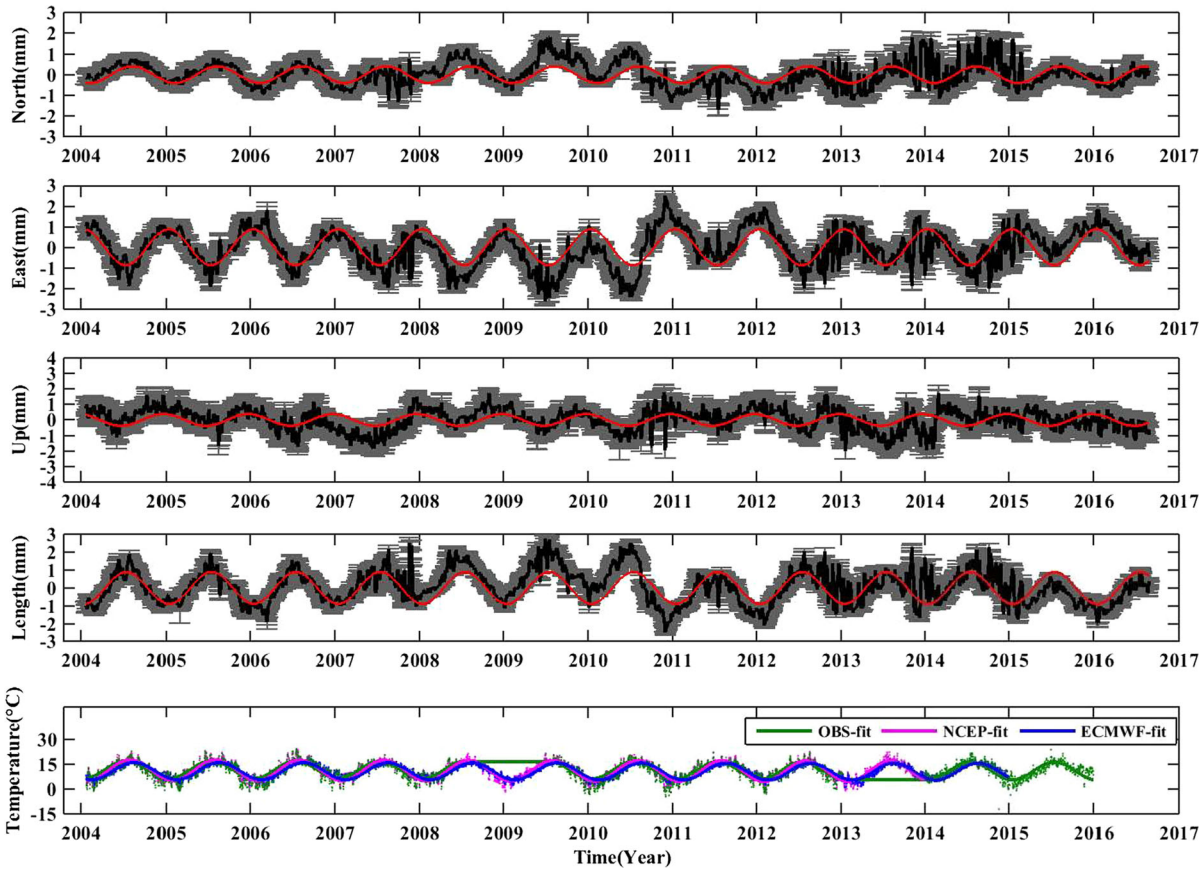

Figure 4
GPS position time series of baseline HEHE (length: 136 m) and the temperature data

2 times greater on the E component than on the U component. This indicates that the site-specific signals or errors may have a greater influence on the horizontal than the vertical direction in GPS position time series.

For the phases, the GPS position time series for each component of the short-baselines have similar characteristics in the time domain; the time series reach a extremum in January (winter) or in July (summer). For the control group, there is no obvious variation in the phase estimates. Given the result in Figs. 1, 2, 3, 4, 5, 6, and 7 show that the GPS position time series of the short-baselines are in phase with the temperature data recorded at each site, we estimated the annual amplitude and phase of the local temperature time series listed in Table 3. The results show that for the baselines in the experimental group, 78% (14/18) of the components have seasonal variations coincident with the local temperature time series with a phase delay within $\pm$ 15° (when the phase delay between the two series is approximately 180°, we consider the variation as the same because the direction of each component can be reversed by simply changing the reference station).

For stations MCCR and CRAR, we failed to obtain the actual local temperature dataset from SOPAC, so the numerical models from the NCEP reanalysis dataset and ECMWF are adopted instead. The two numerical models have a spatial resolution of 2.5° $\times$ 2.5° and a time resolution of one day. The land surface temperature time series are then obtained by linear interpolation. The results indicate that the land surface temperature time series derived from the two numerical models are consistent with the local temperatures recorded for the remainder of the seven short-baselines with acceptable discrepancies. We

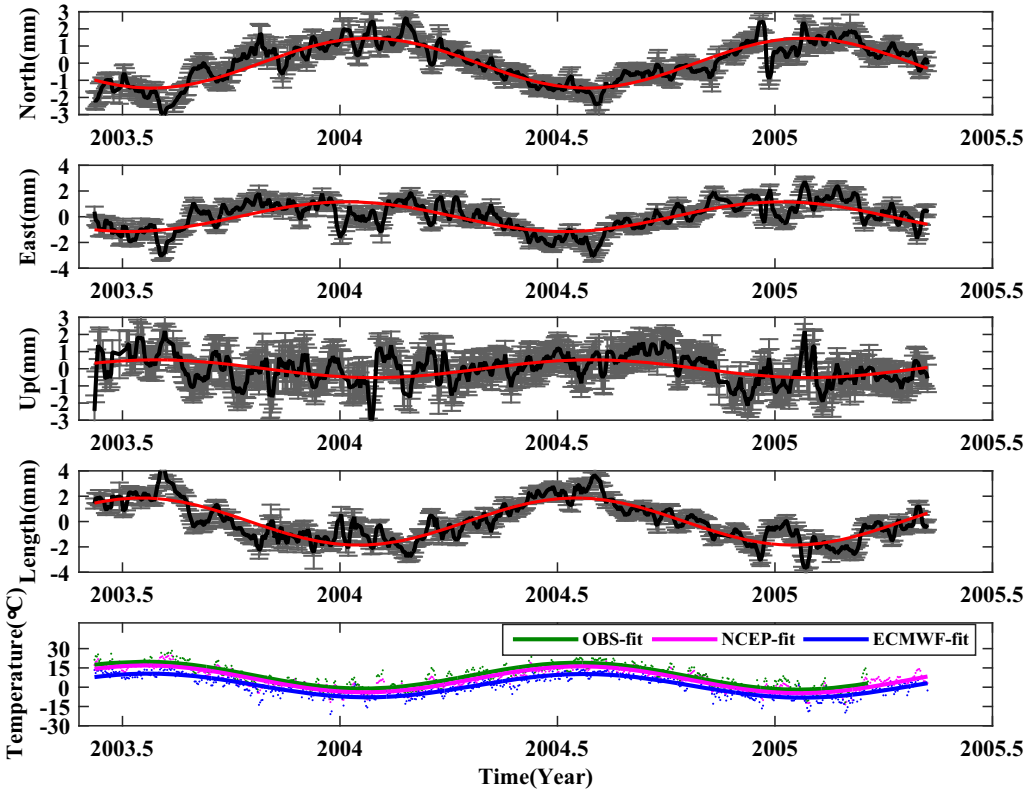

Figure 5
GPS position time series of baseline OBOB (length: 268 m) and the temperature data

note that the annual amplitudes of the GPS position time series of baselines JOJO and MCCR, which have larger annual temperature variations, are much larger than those of the other baselines, whereas for baseline HEHE, which has the smallest annual amplitude of the GPS solutions, the annual temperature variation is only half to one-third that of the other baselines. Similar circumstances occur for baselines with larger differences in the monument height. This indicates that the annual temperature, along with differences in the height or type of monument, may contribute to the seasonal variations in GPS position time series, which will be discussed in detail in Sect. 4.

These results appear to be consistent with those derived by other studies. For example, for baseline HEHE, obvious seasonal signals are observed in our test with annual (semiannual) amplitudes of 0.40 ± 0.06 (0.04 ± 0.18), 0.96 ± 0.07 (0.11 ± 0.06) and 0.41 ± 0.06 (0.14 ± 0.04) mm for the N, E, and U components, respectively. Approximate amplitudes of seasonal oscillations have also been estimated for baselines ZIZI and JOJO (King and Williams 2009; Wilkinson et al. 2013), except for the U components, which both have differences of ~ 0.4 mm. Regardless of the slight difference in GPS processing strategy, the discrepancy is related to the GPS observation span we adopted. The time spans used in this paper for baselines HEHE, ZIZI, and JOJO are 3.4, 2.2 and 3.5 times longer than those used in King and Williams (2009), respectively, which may reduce the formal error for the estimated seasonal amplitude. On the other hand, only the power law and FOGM models were adopted by King and Williams (2009) to study the stochastic noise characteristics of the residuals. BP noise and several combinations are also adopted in this paper, which may result in discrepancies in the estimated uncertainty. Despite these factors, the GPS short-baseline solutions and amplitude estimates of the seasonal signal in this paper are consistent with those in previous studies (King and Williams 2009; Wilkinson et al. 2013) as shown in Table 5.

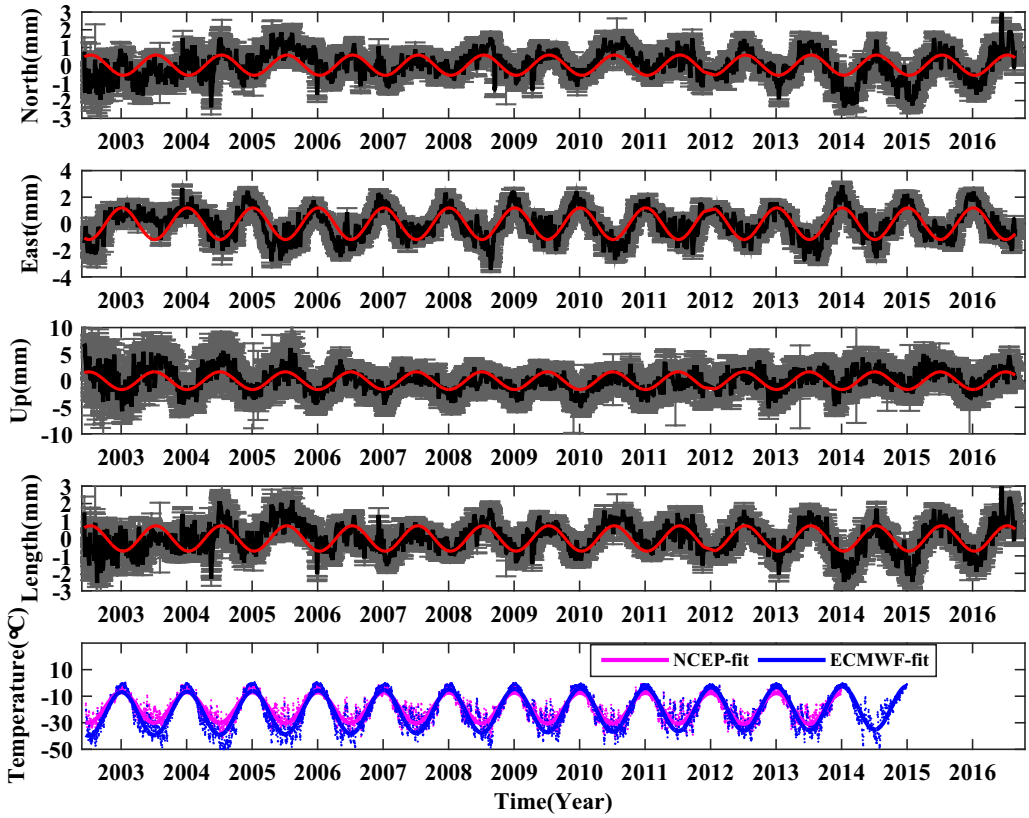

Figure 6
GPS position time series of baseline MCCR (length: 1100 m) and the temperature data

In addition to the seasonal cycles, apparent inter-annual signals are also observed in the GPS baseline time series, such as on the N and U components of baseline JOJO and the E and U components of baseline ZIZI, which have less scattered oscillations. The signals occur every December to the February of the following year and have a maximum oscillation of 8 mm. The origin of this signal will be discussed in detail in Sect. 4.1.

4. *The Origins of the Seasonal Signals in GPS Short-Baseline Time Series*

Because the distances of most of the short-baselines adopted in this paper are less than 1 km, most of the common mode errors are differenced in the GPS solutions, and site-specific signals or errors remain. The potential contributors to the seasonal signals include the TEM, the tropospheric delay error, multipath and other unmodeled factors. Although multipath is one of the main error sources in precise GPS data processing, a detailed simulation by King and Williams (2009) indicates that its impact on the seasonal signal in GPS position time series is limited for short-baselines ZIZI, JOJO and HEHE. Similar results were obtained by Wilkinson et al. (2013), who found that multipath within site HERS was not the source of the seasonal signals. A comparison of the prominent seasonal signal observed in components of the short baselines in the experimental group with the negligible magnitude of the seasonal signal in the control group shows that the difference may be related to the large difference in the monument heights. Interestingly, although there is almost no difference in monument heights for baselines TCTN and RERE, whose antennas are located on the roof of the same building, their annual amplitudes vary (0.42 ± 0.03, 0.36 ± 0.05, and 0.17 ± 0.03 mm for the N, E, and U components of baseline TCTN,

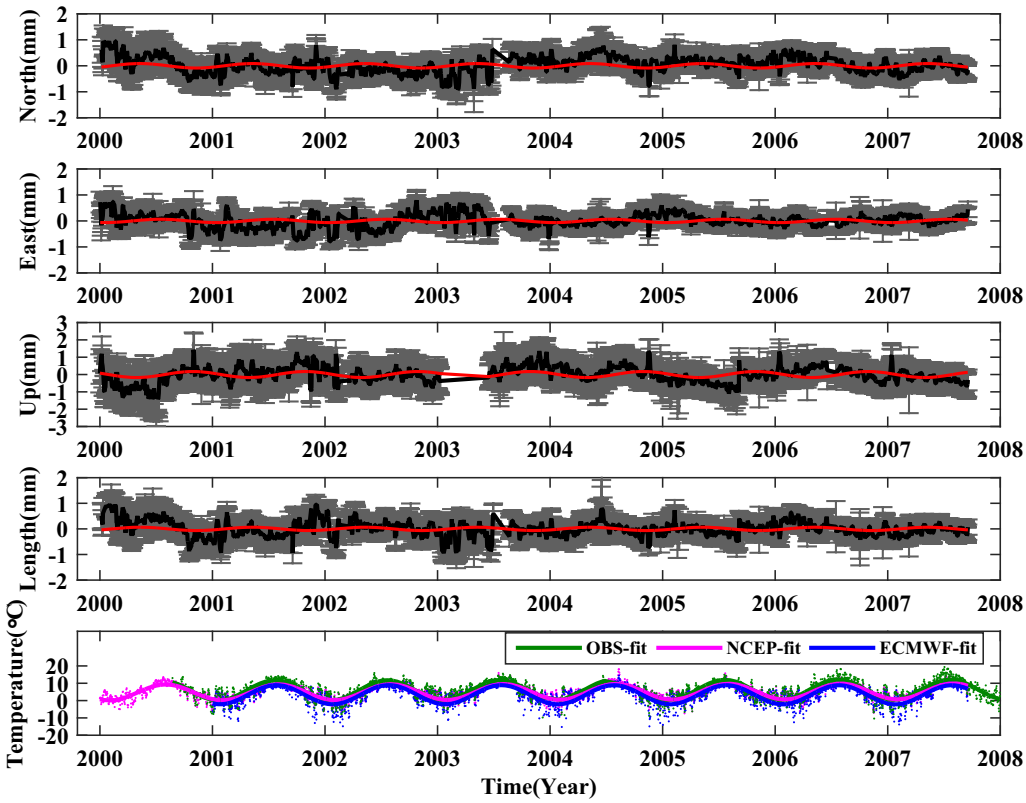

Figure 7
GPS position time series of baseline RERE (length: < 1 m) and the temperature data

respectively, and 0.14 ± 0.10, 0.10 ± 0.18, and 0.28 ± 0.19 mm for the *N*, *E*, and *U* components of baseline RERE, respectively), especially in the vertical direction. This may be caused by the difference between the monument structures of IGS stations TCMS and TNML (see auxiliary material 6).

Given the large differences in monument height, type and structure for the short-baselines adopted in this paper, site-specific signal related to the monuments may be the dominant contributors to the observed seasonal signals. Thus, only the impact of TEM and tropospheric delay error will be discussed in this section.

4.1. Thermal Expansion of the Monument and the Bedrock

Thermally induced deformations of the GPS monument and the bedrock beneath the monument induced by seasonal temperature variations are the main contributors to the seasonal signals in GPS coordinate time series (Dong et al. 2002; Prawirodirdjo et al. 2006; Yan et al. 2009; Munekane 2013; Fang et al. 2014), especially for stations with higher monuments and those that are located in the middle or high latitudes with large daily or seasonal temperature oscillations. Considering the strong correlation between the GPS short-baseline solutions and the local temperature time series shown in Figs. 1, 2, 3, 4, 5, 6, and 7, it is necessary to estimate the contributions of the thermal expansion of the monument itself and bedrock beneath it, which are both closely related to the local temperature.

4.1.1 Contribution to the Vertical Seasonal Signal

The vertical and horizontal directions are discussed separately in this section. The seasonal signals induced by the real seasonal changes of TEM and TEB mainly occur on the vertical component. In the

Table 2

Linear trend and residual RMS estimates of each short-baseline

Baseline	Linear trend (mm/year)[a]				Residual RMS (mm)			
	N	*E*	*U*	*L*	*N*	*E*	*U*	*L*
TCTN	− 0.14 ± 0.00	− 0.06 ± 0.01	0.12 ± 0.02	0.08 ± 0.00	0.2	0.2	0.3	0.3
ZIZI	− 0.10 ± 0.02	− 0.01 ± 0.02	0.26 ± 0.02	0.06 ± 0.02	1.2	1.2	1.0	1.1
JOJO	0.07 ± 0.00	0.10 ± 0.01	− 0.23 ± 0.01	− 0.09 ± 0.01	0.6	1.8	1.7	1.2
HEHE	− 0.24 ± 0.00	0.23 ± 0.01	0.41 ± 0.01	− 0.24 ± 0.01	0.7	0.8	1.0	0.8
OBOB	0.32 ± 0.12	0.01 ± 0.17	− 0.36 ± 0.19	− 0.27 ± 0.17	0.8	1.1	1.3	1.2
MCCR	− 0.74 ± 0.01	0.39 ± 0.01	− 0.04 ± 0.02	− 0.73 ± 0.01	0.8	0.9	2.4	0.8
RERE	0.26 ± 0.01	− 0.07 ± 0.01	0.43 ± 0.02	0.21 ± 0.01	0.6	0.7	1.2	0.7

[a]Uncertainties are 2-sigma errors with 95% confidence from corresponding noise models for the component of each baseline described in Sect. 3.3

Table 3

Statistics of the ONM and estimated relevant parameters

Baseline	TCTN	ZIZI	JOJO	HEHE	OBOB	MCCR	RERE
N							
ONM[a]	PL	BPPL	FL	FOGMRW	BPRW	FL	RW
A.CN[b]	PL: 0.79 ± 0.05	BP: 0.12 ± 0.01 PL: 2.62 ± 0.11	FL: 1.66 ± 0.31	FOGM: 9.90 ± 0.27 RW: 0.86 ± 0.09	BP: 4.79 ± 0.72 RW: 0.00 ± 0.00	FL: 1.74 ± 0.13	RW: 0.54 ± 0.18
A.WN	0.10 ± 0.02	0.00 ± 0.00	3.69 ± 0.04	0.34 ± 0.01	2.12 ± 0.06	1.47 ± 0.02	3.11 ± 0.04
NP[c]	Index: − 1.15	Index: − 1.01	Index: − 1	Beta: 206.04	*F*: 4.32 *W*: 0.70 *N*: − 7.26	Index: − 1	Index: − 2
	TCTN	ZIZI	JOJO	HEHE	OBOB	MCCR	RERE
E							
ONM[a]	FLRW	FOGMRW	FL	FL	BPRW	PL	RW
A.CN[b]	FL: 0.71 ± 0.03 RW: 0.23 ± 0.05	FOGM: 20.92 ± 0.68 RW: 0.69 ± 0.16	FL: 4.40 ± 0.29	FL: 1.90 ± 0.13	BP: 0.10 ± 0.01 RW: 0.00 ± 0.00	PL: 4.05 ± 0.04	RW: 1.00 ± 0.29
A.WN	0.20 ± 0.01	0.60 ± 0.04	2.52 ± 0.04	1.37 ± 0.02	1.15 ± 0.04	0	5.79 ± 0.08
NP[c]	–	Beta: 166.9	Index: − 1	Index: − 1	*F*: 2.46 *W*: 0.05 *N*: 3.13	Index: − 0.11	Index: − 2
	TCTN	ZIZI	JOJO	HEHE	OBOB	MCCR	RERE
U							
ONM[a]	FLRW	BPPL	BPPL	FOGMRW	BPRW	PL	BPRW
A.CN[b]	FL: 0.53 ± 0.02 RW: 0.17 ± 0.05	BP: 0.11 ± 0.01 PL: 4.01 ± 0.19	BP: 0.61 ± 0.09 PL: 7.92 ± 1.65	FOGM: 10.99 ± 0.54 RW: 0.94 ± 0.10	BP: 0.37 ± 0.05 RW: 0.00 ± 0.00	PL: 0.01 ± 0.00	BP: 1.89 ± 0.21 RW: 5.77 ± 0.65
A.WN	0.16 ± 0.02	0.00 ± 0.00	1.23 ± 4.31	0.81 ± 0.02	1.86 ± 0.06	7.05 ± 0.07	3.98 ± 0.06
NP[c]	–	Index: − 1.01	Index: − 0.27	Beta: 224.63	*F*: 3.47 *W*: 0.25 *N*: − 4.90	Index: − 6.05	*F*: 0.45 W: 0.34 *N*: 2.96

[a]All noise models contain white noise

[b]Amplitude of the colored noise (mm)

[c]Estimated relevant noise parameters, including the spectral index of the PL noise, beta of the FOGM noise, and frequency, width, and *n* poles of the BP noise

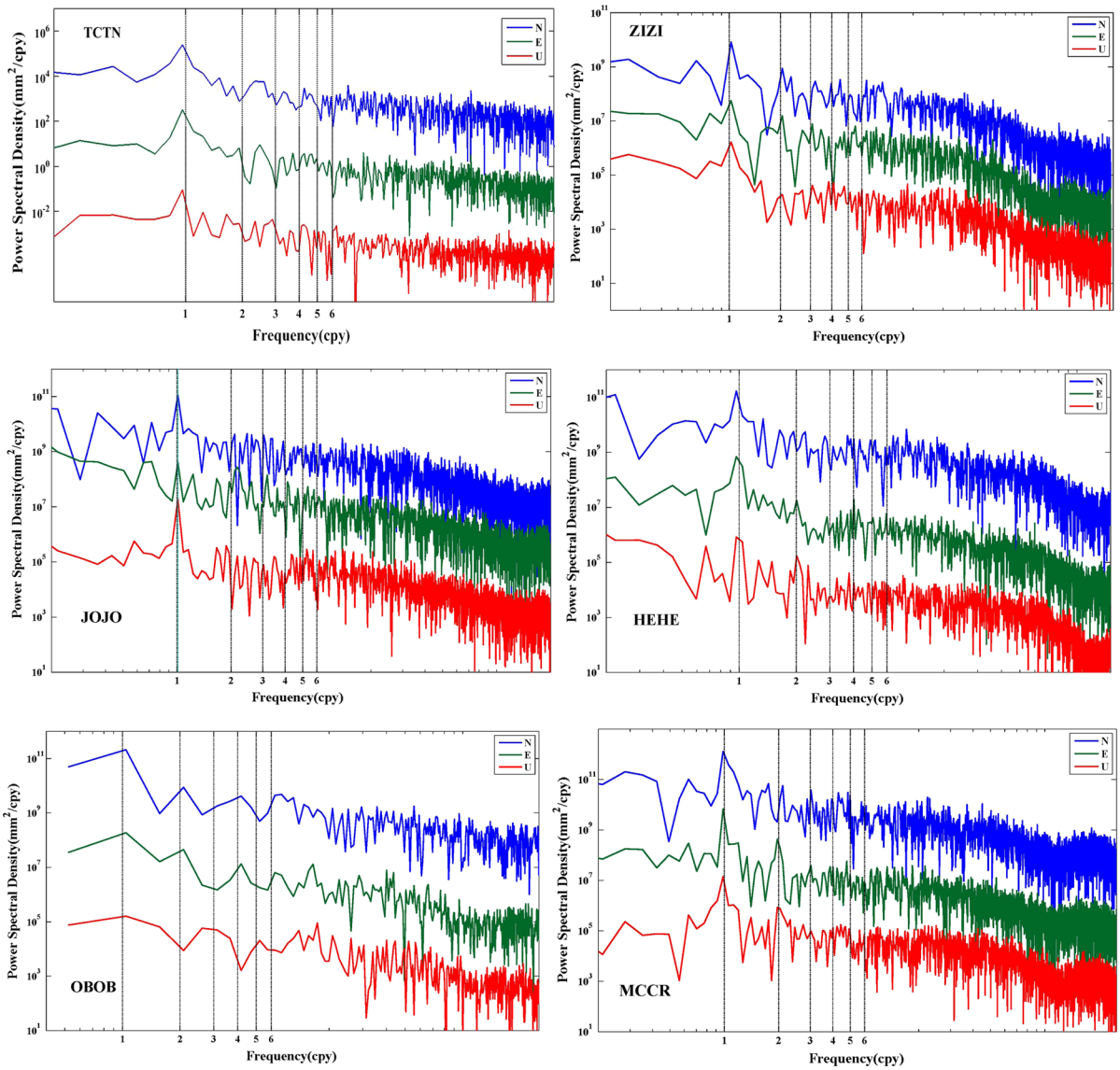

Figure 8
Power spectral density (PSD) values for each component of the baselines in the experimental group. The blue, green and red solid lines are the PSD values of the *N*, *E* and *U* components, respectively, and the gray dotted lines are harmonics of the annual signal. The PSD values for the *N* and *E* components are isolated by adopting appropriate scale factors

horizontal direction, the impact of TEM will be counteracted by the homogeneous geometric characteristics of most of the GPS monuments (except for station in which the monument is attached to one side of a concrete structure on one side; Schenewerk et al. 1999). The TEB displacements of the station pairs for a short-baseline are almost identical due to the slight difference in the temperature gradient in the horizontal direction over such a short distance, but we still estimate the TEB displacement for the single station of each baseline separately considering the slight difference in bedrock conditions underground. The displacements of TEM and TEB are considered and estimated only in the vertical direction in this section.

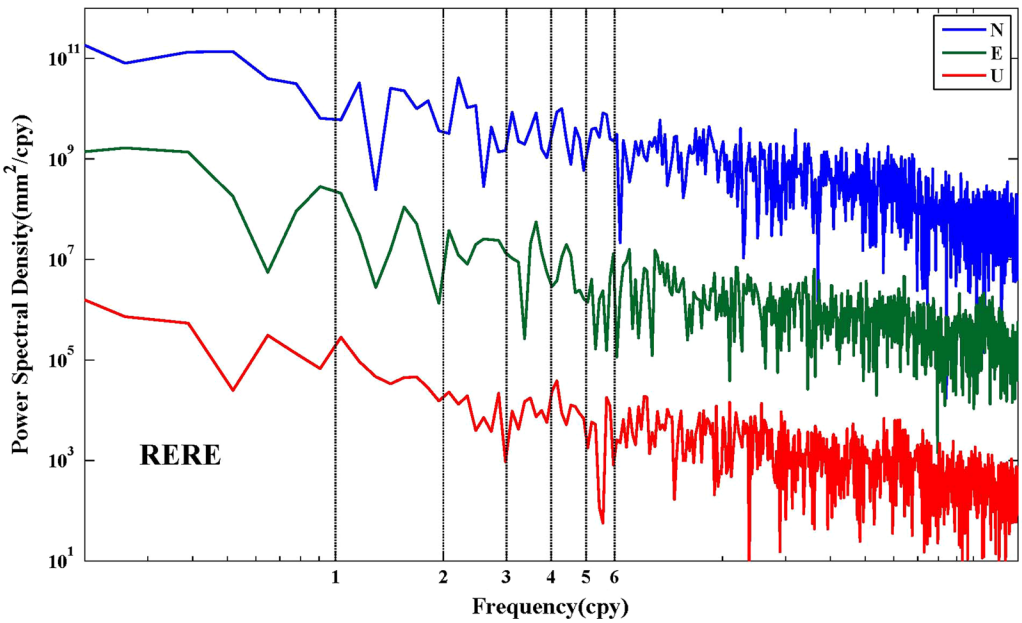

Figure 9
PSD values for the 'zero-baseline' in the control group for comparison

Table 4

Amplitudes and phases estimates for GPS time series and local temperature time series

Baseline		Annual amplitude (mm)	Annual phase (°)	Semi-annual amplitude (mm)	Semi-annual phase (°)	Annual temperature variation (°C)	Annual temperature phase (°)
TCTN	*N*	0.42 ± 0.03	*146 ± 4**	0.05 ± 0.02	− 19 ± 23	7.0 ± 0.1	152 ± 1
	E	0.36 ± 0.05	172 ± 5*	0.04 ± 0.02	− 25 ± 27		
	U	0.17 ± 0.03	76 ± 9	0.00 ± 0.00	–		
	L	0.51 ± 0.03	*155 ± 5**	–	–		
ZIZI	*N*	**1.04 ± 0.13**	*174 ± 7**	0.24 ± 0.13	− 50 ± 24	9.5 ± 0.2	162 ± 1
	E	0.63 ± 0.10	*174 ± 8**	0.34 ± 0.08	− 30 ± 13		
	U	1.04 ± 0.20	*166 ± 11*	0.20 ± 0.14	26 ± 40		
	L	0.11 ± 0.14	*172 ± 8**	–	–		
JOJO	*N*	0.29 ± 0.10	134 ± 19	0.14 ± 0.44	− 39 ± 35	11.3 ± 0.2	165 ± 1
	E	0.39 ± 0.16	*160 ± 24**	0.12 ± 0.12	− 32 ± 57		
	U	**1.86 ± 0.17**	*170 ± 5**	0.97 ± 0.25	− 46 ± 15		
	L	0.41 ± 0.15	*178 ± 17*	–	–		
HEHE	*N*	0.40 ± 0.06	142 ± 8	0.04 ± 0.18	50 ± 45	5.4 ± 1.9	167 ± 21
	E	**0.96 ± 0.07**	*173 ± 4**	0.11 ± 0.06	− 42 ± 30		
	U	0.41 ± 0.06	194 ± 6*	0.14 ± 0.04	− 22 ± 17		
	L	**0.92 ± 0.05**	*168 ± 2*	–	–		
OBOB	*N*	**1.17 ± 0.13**	*155 ± 6**	0.43 ± 0.13	− 6 ± 22	10.2 ± 0.5	162 ± 3
	E	**1.18 ± 0.12**	*175 ± 6**	0.48 ± 0.12	− 24 ± 14		
	U	0.65 ± 0.16	*155 ± 14*	0.28 ± 0.15	− 22 ± 14		
	L	**1.86 ± 0.13**	*165 ± 8*	–	–		
MCCR	*N*	0.59 ± 0.03	*346 ± 3**	0.05 ± 0.06	− 7 ± 39	16.4 ± 0.3	357 ± 1 (South)
	E	**1.32 ± 0.07**	*355 ± 3*	0.39 ± 0.07	47 ± 10		
	U	**1.62 ± 0.14**	*358 ± 5**	0.71 ± 0.14	− 10 ± 12		
	L	0.73 ± 0.08	*349 ± 3**	–	–		

Table 4 *continued*

Baseline		Annual amplitude (mm)	Annual phase (°)	Semi-annual amplitude (mm)	Semi-annual phase (°)	Annual temperature variation (°C)	Annual temperature phase (°)
RERE	*N*	0.14 ± 0.10	10 ± 39	0.12 ± 0.21	− 6 ± 43	5.8 ± 0.2	161 ± 2
	E	0.10 ± 0.18	44 ± 11	0.12 ± 0.16	− 32 ± 81		
	U	0.28 ± 0.19	83 ± 37	0.15 ± 0.24	− 42 ± 27		
	L	0.08 ± 0.09	149 ± 29	–	–		

Bold values indicate significant larger amplitudes than other components

*Phase estimates whose baseline directions are inverted, and the component in italics indicates that the difference of the corresponding phase estimates and the temperature time series is less than 15°

Table 5

Comparison of the amplitude estimates of the seasonal signal for each component

Baseline	Components		King and Williams (2009)	Wilkinson et al. (2013)	This paper
HEHE	Annual	*N*	0.54 ± 0.10	0.50 ± 0.01	0.40 ± 0.06
		E	1.04 ± 0.16	1.05 ± 0.01	0.96 ± 0.07
		U	0.30 ± 0.22	0.42 ± 0.00	0.41 ± 0.06
	Semi-annual	*N*	0.03 ± 0.08	–	0.04 ± 0.18
		E	0.20 ± 0.12	–	0.11 ± 0.06
		U	0.03 ± 0.16	–	0.14 ± 0.04
ZIZI	Annual	*N*	1.08 ± 1.46	–	1.04 ± 0.13
		E	0.59 ± 1.34	–	0.63 ± 0.10
		U	0.68 ± 0.38	–	1.04 ± 0.20
	Semi-annual	*N*	0.29 ± 0.88	–	0.24 ± 0.13
		E	0.30 ± 0.80	–	0.34 ± 0.08
		U	0.21 ± 0.28	–	0.20 ± 0.14
JOJO	Annual	*N*	0.17 ± 0.14	–	0.29 ± 0.10
		E	0.36 ± 0.18	–	0.39 ± 0.16
		U	2.25 ± 0.92	–	1.86 ± 0.17
	Semi-annual	*N*	0.16 ± 0.10	–	0.14 ± 0.44
		E	0.17 ± 0.12	–	0.12 ± 0.12
		U	0.99 ± 0.56	–	0.97 ± 0.25

The unit of numbers are millimeters

Previous studies estimate the displacement associated with the TEM with a simple linear expansion model that consists of three main parameters: the linear expansion coefficient (which depends on the monument's material), the monument height and the temperature variation (observed in the M-file). However, only part of the seasonal signal observed in the vertical direction can be well explained by the TEM, and the ratio of the modeled TEM amplitude to the observed GPS amplitude is 1.88 for baseline HEHE (King and Williams 2009). This result may be biased by the estimated seasonal amplitude and/or the TEM model adopted. Hence, we re-estimated the seasonal terms with longer GPS observations in Sect. 3.3. The monument heights in Sect. 2.1 which are used in the TEM model were updated by considering the additional parts of the monument, including the building under the monument and the shallow underground part of the monument. The monuments of numerous GPS stations are mounted on the edges of roofs to obtain better satellite visibility and stability. However, the buildings that support the monument will also deform due to seasonal temperature variations, especially the edges of structures, which are sensitive to direct solar heating (Santamaría-Gómez 2013). In contrast, some GPS monuments are affixed directly onto the bedrock (e.g. site ZIMM has an underground depth of $\sim$ 1.5 m above the bedrock). The shallow underground part of the monument may also deform with the seasonal variation of the surface temperature. Hence, the length of the annex building and the shallow

underground part of the monument are considered simultaneously when estimating the TEM with the linear expansion model. Due to the small order of magnitude of TEB for the station pairs of each short-baseline (which have nearly identical bedrock conditions), we adopted the half-space model derived by Dong et al. (2002) and extended by Yan et al. (2009) with analytical solutions to estimate the TEB displacements in the vertical direction, instead of using the three-dimensional uniform spherical model proposed by Fang et al. (2014).

Figure 10 shows the modeled thermal expansion (MTE, which is the sum of TEM and TEB) displacements and the observed GPS height time series for each short-baseline. Table 6 shows the corresponding amplitudes and phases estimated from these time series. The modeled TEM displacements are somewhat continuous because the input local temperature time series are not available for every day. The results indicate that the modeled and observed time series for these short-baselines are consistent with each other in the time domain. The annual oscillations are nearly identical, especially for baselines ZIZI, JOJO, OBOB and MCCR, whereas for baseline HEHE, there is a phase delay between the MTE displacements and the observed GPS solutions. The results of the estimated amplitudes and phases verify the good agreement. For example, for baseline ZIZI, the annual amplitudes of the observed GPS baseline heights and the TEM and TEB displacements are 1.04 ± 0.20, 0.86 ± 0.01 and 0.16 ± 0.00 mm, respectively, with annual phases of $-14° \pm 11°$, $-18° \pm 1°$ and $-63° \pm 0°$, respectively. The median annual amplitude ratio of the TEM to the observed GPS heights is $\sim 88\%$ for the baselines in the experimental group, and almost all of the annual phase delays between the TEM and the observed GPS heights are within $\pm 6°$ except for baselines TCTN and HEHE. The contribution of the TEM to the observed GPS heights for the semi-annual oscillation is not as prominent as in the annual signal, with average amplitude ratios of $\sim 9\%$. There also appears to be no significant correlation between the semi-annual phases. For baseline MCCR, the monument of station MCM4 is attached directly to the bedrock, and its height is approximately 0 m when estimating the TEM. This indicates that the seasonal signal that exists in the baseline time series of MCCR, especially in the vertical direction, is likely related to the thermally induced deformation of the GPS monument of station CRAR. For baseline OBOB, the ratio of the amplitudes exceeds 1, which means that the TEM amplitude is slightly greater than that of the observed GPS. Considering the uncertainty in the amplitudes of the observed GPS heights, this ratio is reasonable. The close relationship between the GPS observations and the modeled TEM may result from the strong correlation between the GPS observations and the local temperature, which is one of the main input datasets of the modeled TEM.

Comparing with results of King and Williams (2009), the ratio of the TEM to the annual amplitude of GPS short-baseline heights in this paper is more significant. This may be explained by: (1) the height difference between the station pairs of the short-baselines we chose in this paper are larger; and (2) the height of the monument itself and where it is attached (e.g., the building for monuments on roofs) are considered in this paper when estimating the modeled TEM. The results indicate that TEM may be the main contributor to the annual signal observed in GPS short-baseline time series, especially in the vertical direction. However, other apparent signals cannot be explained well. For example, for baseline TCTN, the annual amplitude of 0.17 mm cannot be explained by TEM based on the current model because there is only a slight difference in their monument heights (about 20 cm). In addition, the annual amplitudes for TCTN in the horizontal direction are 0.42 ± 0.03 and 0.36 ± 0.05 mm, which are nearly 3 times larger than the amplitudes in the vertical direction. Also, the annual oscillations on the N and U components of baselines ZIZI and JOJO appear to be unrelated to the thermally induced displacements of either the monument or the bedrock. This unusual signal was also observed by King and Williams (2009), but its origin remained unclear. The results in this paper suggest that the periodic oscillations can reach 8 mm from December of each year to the end of February of the following year from 2003 to 2015, which indicates that JOZ2 rose or JOZE settled to some extent during every winter. This is likely a systematic error which is related to site environment because similar signals were not

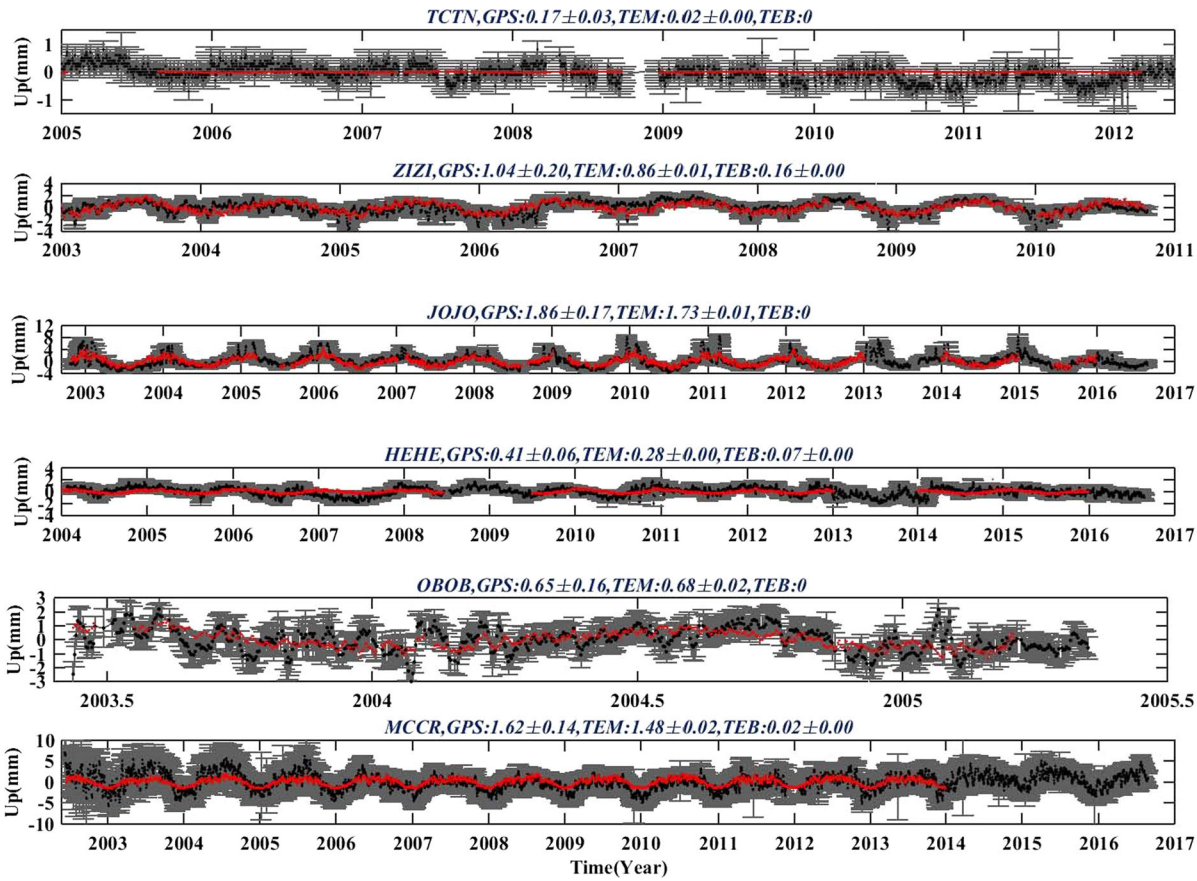

Figure 10
MTE displacements and observed GPS time series in the vertical direction for each short-baseline. The red line represents the MTE displacements (TEM + TEB), and the corresponding annual amplitudes and phases are shown above each sub-graph

Table 6

Amplitude and phase estimates of the MTE displacements and observed GPS time series

Baselines	TCTN	ZIZI	JOJO	HEHE	OBOB	MCCR	RERE
A.A							
U	0.17 ± 0.03	1.04 ± 0.20	1.86 ± 0.17	0.41 ± 0.06	0.65 ± 0.16	1.62 ± 0.14	0.28 ± 0.19
TEM	0.02 ± 0.00	0.86 ± 0.01	1.73 ± 0.01	0.28 ± 0.00	0.68 ± 0.02	1.48 ± 0.02	0
TEB	0	0.16 ± 0.00	0	0.07 ± 0.00	0	0.02 ± 0.00	0
Ratio	11.8%	84.1%	93.0%	70.4%	104.6%	91.4%	0
A.P							
U	76 ± 9	− 14 ± 11	− 10 ± 5	14 ± 9	− 25 ± 14	− 20 ± 5	83 ± 37
TEM	− 20 ± 1	− 18 ± 1	− 13 ± 2	− 25 ± 1	− 19 ± 1	− 23 ± 1	0
TEB	0	− 63 ± 0	0	− 70 ± 0	0	0	0
S.A.A							
U	0.00 ± 0.00	0.20 ± 0.14	0.97 ± 0.25	0.14 ± 0.04	0.28 ± 0.15	0.71 ± 0.14	0.15 ± 0.24
TEM	0	0.02 ± 0.01	0.07 ± 0.08	0.01 ± 0.01	0.06 ± 0.03	0.18 ± 0.02	0
TEB	0	0	0	0	0	0	0
Ratio	–	10.0%	7.2%	7.1%	21.4%	25.4%	0
S.A.P							
U	–	26 ± 40	− 46 ± 15	− 22 ± 16	− 22 ± 14	− 10 ± 12	− 42 ± 27

Table 6 *continued*

Baselines	TCTN	ZIZI	JOJO	HEHE	OBOB	MCCR	RERE
TEM	–	59 ± 34	74 ± 24	− 76 ± 12	− 52 ± 15	− 14 ± 2	0
TEB	–	0	0	0	0	0	0

observed in other short-baseline solutions except for ZIZI and JOJO. Apparent oscillations also appeared in the PPP solutions of station ZIMM when the GPS antenna was covered by thick snow during December (Wu 2012) and may be induced by signal delay error. The position error can be a few centimeters in both the horizontal and vertical directions. It is proposed that the oscillation observed in this paper was also caused by a similar factor. Another possible reason may be the temperature difference inside and outside the building that support the antenna. The ambient temperature difference is usually lower than − 20° during the winter, which may lead to unexpected deformations especially on the *U* component. But unfortunately, the variation is not well modeled by the TEM model because the air temperature data we adopted are inconsistent with the actual inner temperature of the building. Although the annual signal in the vertical direction for most short-baselines can be explained by TEM and TEB, the origin of the seasonal signals in the horizontal direction needs to be investigated further.

4.1.2 Propagation of Daily/Sub-Daily Signal to the Horizontal Signal

Although the seasonal signal observed in the vertical direction can be well explained by TEM and TEB, the origins of the annual and semi-annual cycles in the horizontal direction require further discussion. For baseline RERE, the GPS antennas are located only a few meters away from each other (seen in the auxiliary material 6). According to the log file, they are anchored into the concrete of the balustrade wall at the top of the elevator tower in the same building. The building is ∼ 12 m high and has a ∼ 21 m foundation deeply into the bedrock. Similarly, the GPS antennas for baseline TCTN are also anchored into the roof of a concrete building. However, they have quite different monument structures; one is a steel truss, and the other is a steel mast. This strongly suggests that the thermally induced displacements of the monuments may be responsible for the annual amplitude difference of baseline TCTN and RERE, especially in the horizontal direction.

According to previous studies, mismodeled geophysical signals (such as atmospheric loading) or systematic errors (such as errors induced by satellite orbits, multipath or phase center variations) may introduce sub-seasonal cycles around K1, K2, S1 and S2 in GPS station time series, which can propagate into annual or semi-annual signal during precise data processing procedures (Stewart et al. 2005; Penna et al. 2007), especially for 24-h batch solutions (King et al. 2008; King and Williams 2009). In addition, daily or sub-daily displacements induced by TEM due to periodical temperature variations may also propagate to annual or semi-annual signals in GPS daily solutions (Munekane 2013), especially for the GPS stations with higher monuments or with large seasonal temperature variations adopted in this paper.

The analysis of GPS kinematic solutions of GEONET in Japan by Munekane (2012, 2013) indicates that a significant portion of the observed sub-daily displacements in GPS position time series are due to thermal tilts of the GPS monuments. The spectral peaks around the S1 and S2 bands decrease by more than 40% on the *N* and *E* components, respectively, after applying the TEM corrections. The deformation is opposite to the direction of the sun, and it mainly occurs during the daytime with sufficient sunlight and reverses during the evening or on cloudy days. Similarly, an integrated test applied by Lehner (2011) in a high latitude area indicates that for a steel truss monument with a height of 3.2 m (shown in Fig. 11, which has analogous structure to the monuments of stations ZIMM, HERS and CRAR in this paper), the thermally induced monument motion can exceed 1 mm in the horizontal direction even though an insulated pipe was installed to prevent direct heating by solar radiation. For a deeply braced and consolidated steel mast monument

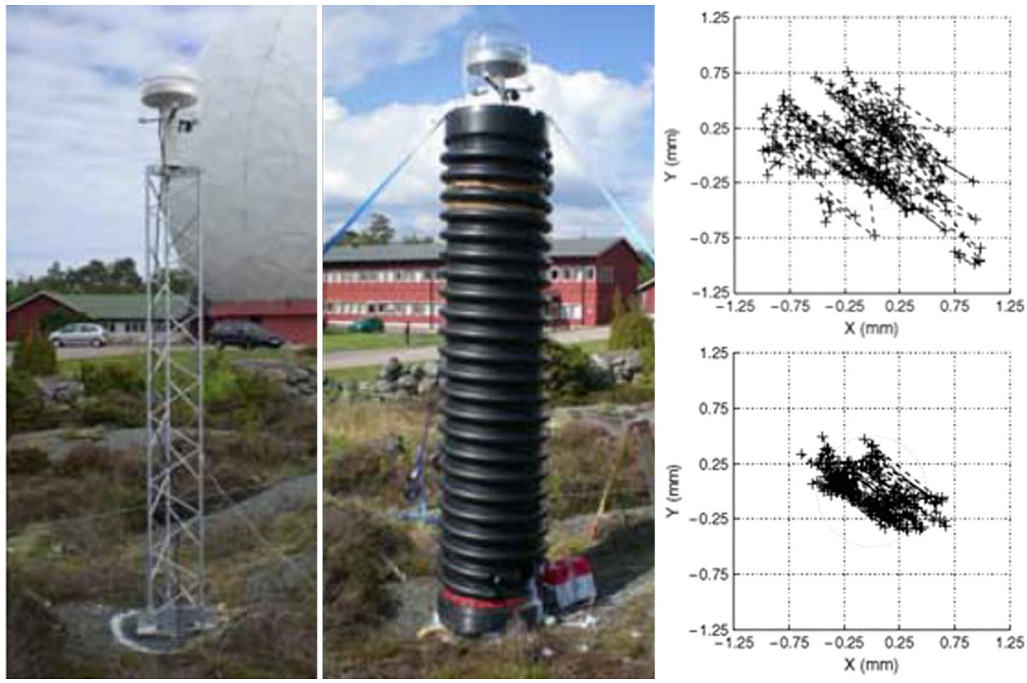

Figure 11
Steel truss monuments with and without insulated pipes (from Lehner 2011). The two graphs on the right show the thermally induced deformation in the horizontal direction that corresponds to the monument in the left panel

with a triangular attachment set directly onto the bedrock with approximate length (not shown), the daily thermally induced monument motion can reach 3 mm during the summer (Haas et al. 2013). These daily or sub-daily monument motions are likely a result of thermally induced deformation of the elastic material due to direct solar radiation.

Although no other independent observations, such as thermal tilts or total station, were adopted in the short-baselines in this paper, we believe that the thermally induced displacements of the GPS monuments in these short-baselines can exhibit sub-seasonal periodical characteristics around the S1 and S2 bands for two reasons. One reason is that almost all of the short-baselines in the experimental group have monument height differences greater than 5 m (except for TCTN, which has obvious differences in the monument structures), which is equivalent to the monument heights of the GPS stations adopted in Munekane (2013). The other reason is that almost all of the GPS station pairs of the short-baselines in the experimental group (except for TCTN, which has the smallest observed annual amplitude) are located in middle- or high- latitude areas with apparent seasonal and daily temperature variations. For example, according to the observed local temperatures recorded in the M-file of JOZE, the temperature variation in a single day (the 222nd day of year 2015) was 11.3 °C. The change will be greater if heating by solar radiation is taken into account. Considering the fact that the GPS solutions are processed in 24-h batches, these daily or sub-daily thermally induced deformations of the monument may also propagate into spurious long-term signals such as annual and semi-annual terms in GPS short-baseline position time series (Penna and Stewart, 2003; Penna et al. 2007; King et al. 2008). However, pure modeling of the thermally induced displacement of the GPS monuments with different heights, types and structures still requires further investigation.

4.2. *Tropospheric Delay*

The tropospheric delay is one of the main error sources in precise GPS processing that can reduce the accuracy of the daily solutions (Boehm et al. 2006).

The error induced by mismodeling of the tropospheric delay can also propagate into GPS short-baseline position time series (Munekane and Boehm 2010), especially for baselines with large height differences (Schön 2006).

Thus, to investigate the tropospheric delay error and its impact on GPS short-baseline position time series, GPS observations of baselines MCCR (which has a height difference of $\sim$ 120 m) and PEPE (short for PETS-PETP, which has a baseline length of 5600 m and a height difference of $\sim$ 110 m) are adopted and processed with and without considering the tropospheric zenith delay. The IGS station PETS is located on a hill in Kamchatka, Russian Federation, and station PETP is located on top of a building $\sim$ 5.6 km away. The time span of baseline PEPE is approximately 4.5 years (March 2004 to December 2008). The GPS short-baseline time series of MCCR and PEPE with and without the tropospheric zenith delay are shown in Figs. 12 and 13, respectively. It can be inferred that there is no significant difference between the two strategies for both the *N* and *L* components of the GPS position time series, whereas the discrepancies are much more apparent on the *E* and *U* components. According to the results, the annual amplitude is 5.8 mm in the vertical direction if the tropospheric zenith delay parameters are not estimated for baseline PEPE, and the amplitude decreases to $\sim$ 1 mm when the tropospheric zenith delay parameters are estimated every 2 h. Similar results occur for baseline MCCR on the *U* component, with an annual amplitude difference of $\sim$ 1.84 mm. In other words, there are spurious seasonal signals with annual amplitudes of $\sim$ 5 and $\sim$ 2 mm for baselines PEPE and MCCR, respectively, if the tropospheric delay error is not well or properly modeled. These results indicate that errors induced by mismodeling of the tropospheric zenith delay may contribute to the long-term seasonal signals in GPS short-baseline time series, especially for station pairs with height differences greater than 100 m. In addition, for baseline MCCR, the solutions in the vertical direction are less noisy and have larger formal errors when the tropospheric zenith delay parameters are estimated. Thus, the more scattered time series for May 2002 and November 2005 in Fig. 5 are likely a result of systematic error rather than poor quality of the GPS observations.

In addition to thermal expansion and the tropospheric delay error, other errors related to the GPS

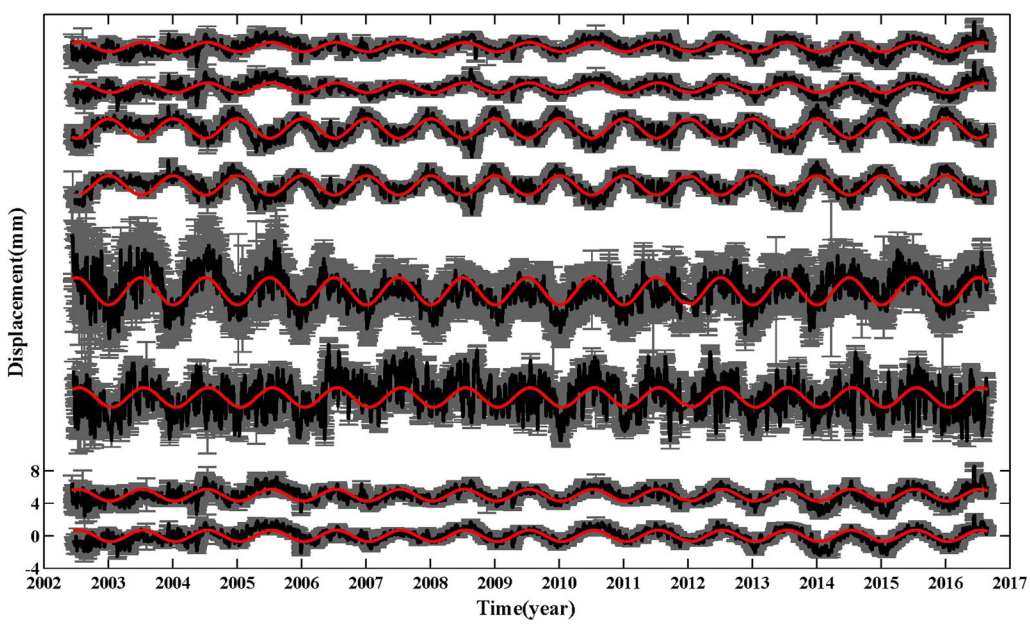

Figure 12
GPS short-baseline residual time series of MCCR with and without considering the tropospheric delay. The time series pairs are the *N*, *E*, *U* and *L* components from top to bottom. The annual signals are fit and shown by the red lines. Offsets are applied to separate the time series

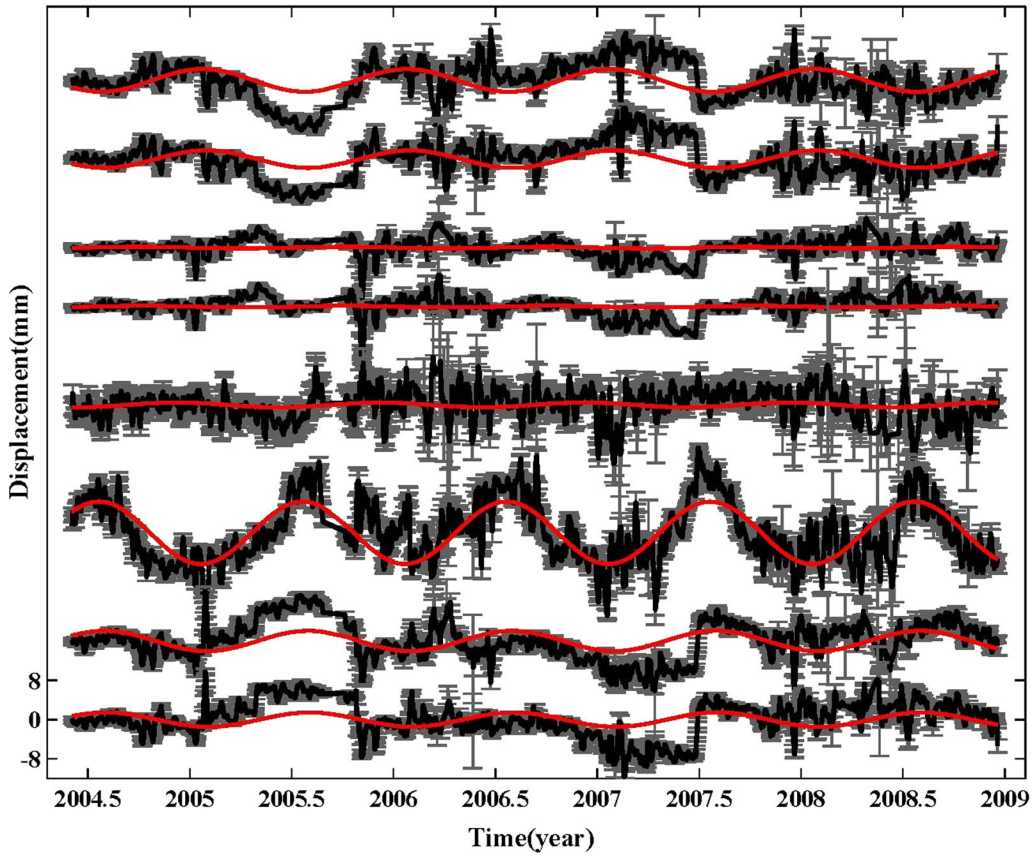

Figure 13
GPS short-baseline residuals of PEPE with and without considering the tropospheric delay

technique or site-specific signals may also contribute to the seasonal signals in the GPS short-baseline time series in this paper, such as errors induced by phase center variations between heterogeneous receivers and antennas or seasonal variations of the local water table for station pairs with longer distances. The aliasing of signals with various origins make the conditions more complicated (Penna and Stewart 2003) and also require further investigation. It should be noted that there might be a slight difference between the 24-h batch session solution adopted in this paper and the kinematic solutions by Track (Herring 2009) derived from King and Williams (2009). The potential unmodeled sub-daily signal (not the thermally induced part) may also propagate into long-term periodical signals, such as annual or semiannual cycles (Penna et al. 2007), which can rarely be captured by the daily solutions and may introduce bias. However, the impact of this difference is limited compared to the apparent seasonal amplitude we have observed. Therefore, the qualitative and quantitative analyses in this paper still provide insight into investigations of the origin of seasonal signals in GPS short-baseline time series.

5. Conclusions

It is necessary to properly model and better understand the seasonal signal in GPS position time series. Quantitative analyses of seasonal signals based on the results of GPS short-baseline time series are more reliable than other results because most GPS systematic errors can be eliminated by differenced and the impacts of common mode geophysical signals on station pairs are nearly identical (King and Williams, 2009; Hill et al. 2009). In this paper, six GPS short-baselines (distances < 1.1 km) and an

approximately 'zero-baseline' (distance < 1 m) were adopted and processed to study the seasonal signals in GPS short-baseline position time series. To ensure that the useful signals from the GPS monuments would not be overwhelmed by other site-specific errors, IGS station pairs of the short-baselines in the experimental group with apparent differences between their GPS monuments (including the height, material type or/and structure of the monument) were chosen. The antennas of the 'zero-baseline' in the control group are affixed to the edge of the same roof, which means that they have identical monuments.

GPS short-baseline solutions for the 6 selected short-baselines show that there are apparent seasonal signals in both the horizontal and vertical directions. The annual amplitudes generally exceed 1 mm, and the maximum amplitude is 1.86 ± 0.17 mm on the vertical component of short-baseline JOJO. For comparison, the annual amplitudes of the 'zero-baseline' with identical monuments are 0.14 ± 0.10, 0.10 ± 0.18, 0.28 ± 0.19 and 0.08 ± 0.09 mm for the N, E, U, and L components, respectively. The amplitudes are generally coincident with those estimated by King and Williams (2009) and Wilkinson et al. (2013) but have much smaller uncertainties, which may be due to the much longer GPS data spans and diversified optimal noise models we adopted. For the time-correlated noise, the ONM varies between the short-baselines. For the baselines in the experimental group, 40 and 20% of the components can be best modeled by BP and FOGM noise, respectively, and the BP noise is much more significant in the vertical direction than in the horizontal direction. For the control group, the stochastic processes for all three components exhibit characteristics of RW, which is similar to the results of the distance meter measurements from Langbein (2004). The discrepancies in the seasonal amplitudes and the ONM between the experimental group and the control group are likely related to the apparent differences between the GPS monuments, such as differences in monument height, type or structure.

The seasonal signals in the GPS short-baseline time series for 78% (14/18) of the components are generally in phase with the recorded local site temperatures in the time domain. We applied a linear thermal expansion model to estimate the impact of TEM on the seasonal signals. The model considered the height of the monument, its annex building, and its underground part simultaneously. The results suggest that the estimated TEM displacements are responsible for $\sim 84\%$ of the observed annual amplitude in the vertical direction for the selected GPS short-baselines, compared to a mean contribution of $\sim 46\%$ for only the geodetic monument. This indicates that the thermally induced deformation of the monuments estimated in this paper may account for a large proportion of the apparent annual signal exhibited in GPS short-baseline position time series, which is an obvious improvement over previous methods.

In addition, annual amplitudes of > 0.4 mm are generally observed in the horizontal direction. The maximum amplitude is 1.32 ± 0.07 mm on baseline MCCR, which is located in Antarctica with apparent daily temperature variations. The horizontal signal cannot well explained by long-term deformation induced by thermal expansion. The daily or sub-daily signals induced by TEM may propagate into the daily GPS short-baseline time series with spurious long-period signals, such as annual or semi-annual cycles, especially in the horizontal direction. In addition, GPS systematic errors, such as the tropospheric delay and signal delay of GPS antenna induced by snow cover, may be potential contributors to the seasonal signals in GPS short-baseline position time series. The spurious annual amplitudes induced by the tropospheric delay error are ~ 5 and ~ 2 mm, respectively, for two short-baselines with height difference greater than 100 m, which should also be taken into account. However, the mechanism of seasonal signals observed in the horizontal direction in GPS short-baseline time series requires additional comprehensive investigations.

Although the geophysical mechanism of seasonal signals in GPS position time series and their quantitative analysis have been illustrated elaborately by recent researches (Davis et al. 2012; Deng et al. 2016; Penna et al. 2007; Johnson et al. 2017; Xu et al. 2017; Wang et al. 2018), it is still difficult to extract or separate variations caused by a single contributor from GPS observations due to the various error/signal sources and their aliasing effects in GPS position time series. However, the results in this paper give another

insight into how thermal effects of the GPS monument and the tropospheric delay errors propagate into geodetic estimations using 'pure' GPS short-baseline observations, in which most of the common systematic errors and large-scale geophysical signal are absent. In additions, conclusions in this paper may also make the performance of GNSS deformation monitoring of large structures (Jiang et al. 2012) or railways (Ma et al. 2016) more reliable based on short-baseline observations once the thermal effect of the monument is taken into account (Chen et al. 2018).

Acknowledgements

We thank the two anonymous for their helpful recommendations. We thank the SOPAC and NCEP/ECMWF for providing raw GPS observations and temperature dataset, respectively. We thank Dr. Williams for providing CATS software package. We also thank Juergen Neumeyer, Thomas Nylen, Gudmundur Valsson, and Ryan Ruddick for providing pictures and information about the IGS stations. This research is supported by the National Science Foundation for Distinguished Young Scholars of China (Grant no. 41525014) and the National Natural Science Foundation of China (Grant nos. 41374033 and 41210006), and the Program for Changjiang Scholars of the Ministry of Education of China. This research is also supported by the project of Wuhan University for overseas exchange graduate.

References

Altamimi, Z., Rebischung, P., Métivier, L., & Collilieux, X. (2016). ITRF2014: A new release of the international terrestrial reference frame modeling nonlinear station motions. *Journal of Geophysical Research: Solid Earth, 121,* 6109–6131.

Blewitt, G., Lavallee, D., Clarke, P., & Nurutdinov, K. (2001). A new global mode of Earth deformation: Seasonal cycle detected. *Science, 294*(5550), 2342–2345.

Boehm, J., Niell, A., Tregoning, P., & Schuh, H. (2006). Global mapping function (GMF): A new empirical mapping function based on numerical weather model data. *Geophysical Research Letters, 33*(7).

Chen, Q., Jiang, W., Meng, X., Jiang, P., Wang, K., Xie, Y., et al. (2018). Vertical deformation monitoring of the suspension bridge tower using GNSS: A case study of the forth road bridge in the UK. *Remote Sensing, 10*(3), 364.

Collilieux, X., Altamimi, Z., Coulot, D., van Dam, T., & Ray, J. (2010). Impact of loading effects on determination of the International Terrestrial Reference Frame. *Advances in Space Research, 45*(1), 144–154.

Davis, J. L., Wernicke, B. P., & Tamisiea, M. E. (2012). On seasonal signals in geodetic time series. *Journal of Geophysical Research: Solid Earth, 117*(B1).

Deng, L., Jiang, W., Li, Z., Chen, H., Wang, K., & Ma, Y. (2016). Assessment of second- and third-order ionospheric effects on regional networks: case study in China with longer CMONOC GPS coordinate time series. *Journal of Geodesy, 91*(2), 207–227.

Dong, D., Fang, P., Bock, Y., Cheng, M. K., & Miyazaki, S. (2002). Anatomy of apparent seasonal variations from GPS-derived site position time series. *Journal of Geophysical Research Atmospheres, 107*(B4), ETG 9-1–ETG 9-16.

Fang, M., Dong, D., & Hager, B. H. (2014). Displacements due to surface temperature variation on a uniform elastic sphere with its centre of mass stationary. *Geophysical Journal International, 196,* 194–203.

Haas, R., Bergstrand, S., & Lehner, W. (2013). Evaluation of GNSS monument stability. In Reference frames for applications in geosciences (pp. 45–50). Berlin: Springer.

Herring, T. A. (2009). *Example of the usage of TRACK*, Massachusetts's Institute Mass., Inst. of Technol., Cambridge. http://geoweb.mit.edu/tah/track_example/.

Herring, T. A., King, R. W., & McClusky, S. C. (2010). *GAMIT reference manual, release 10.4: Cambridge, Massachusetts Institute of Technology Department of Earth, Atmospheric, and Planetary Sciences*, 171 pp.

Hill, E. M., Davis, J. L., Elósegui, P., Wernicke, B. P., Malikowski, & Niemi, E. N. A (2009). Characterization of site-specific GPS errors using a short-baseline network of braced monuments at Yucca Mountain, Southern Nevada. *Journal of Geophysical Research, 114*(B11).

Jiang, W., Liu, H., & Zhou, X. (2012). Analysis of long-term deformation of reservoir using continuous GPS observations. *Acta Geodaetica Et Cartographica Sinica, 41*(5), 682–689.

Johnson, C. W., Fu, Y., & Bürgmann, R. (2017). Stress models of the annual hydrospheric, atmospheric, thermal, and tidal loading cycles on California faults: Perturbation of background stress and changes in seismicity. *Journal of Geophysical Research: Solid Earth, 122,* 10605–10625.

King, M. A., & Watson, C. S. (2010). Long GPS coordinate time series: Multipath and geometry effects. *Journal of Geophysical Research Solid Earth, 115*(B4), 2500–2522.

King, M. A., Watson, C. S., Penna, N. T., & Clarke, P. J. (2008). Sub-daily signals in GPS observations and their effect at semi-annual and annual periods. *Geophysical Research Letters, 35*(3), 247–255.

King, M. A., & Williams, S. D. P. (2009). Apparent stability of GPS monumentation from short-baseline time series. *Journal of Geophysical Research, 114*(B10).

Langbein, J. (2004). Noise in two-color electronic distance meter measurements revisited. *Journal of Geophysical Research: Solid Earth, 109*(B4).

Langbein, J. (2008). Noise in GPS displacement measurements from Southern California and Southern Nevada. *Journal of Geophysical Research, 113*(B5).

Langbein, J. (2012). Estimating rate uncertainty with maximum likelihood: differences between power-law and flicker–random-walk models. *Journal of Geodesy, 86*(9), 775–783.

Leh ner, W. M. (2011). Evaluation of environmental stresses on GNSS-monuments. Master of Science Thesis, Chalmers University of Technology.

Ma, F., Xi, R., & Xu, N. (2016). Analysis of railway subgrade frost heave deformation based on GPS. *Geodesy and Geodynamics, 7*(2), 143–147.

Munekane, H. (2012). Coseismic and early postseismic slips associated with the 2011 off the Pacific coast of Tohoku Earthquake sequence: EOF analysis of GPS kinematic time series(J). *Earth, Planets and Space, 64*(12), 1077–1091.

Munekane, H. (2013). Sub-daily noise in horizontal GPS kinematic time series due to thermal tilt of GPS monuments. *Journal of Geodesy, 87*(4), 393–401.

Munekane, H., & Boehm, J. (2010). Numerical simulation of troposphere-induced errors in GPS-derived geodetic time series over Japan. *Journal of Geodesy, 84*(7), 405–417.

Penna, N. T., King, M. A., & Stewart, M. P. (2007). GPS height time series: Short-period origins of spurious long-period signals, *Journal of Geophysical Research, 112*(B2).

Penna, N. T., & Stewart, M. P. (2003). Aliased tidal signatures in continuous GPS height time series. *Geophysical Research Letters, 30*(23), 69–73.

Prawirodirdjo, L., Ben-Zion, Y., & Bock, Y. (2006). Observation and modeling of thermoelastic strain in southern California integrated GPS network daily position time series. *Journal of Geophysical Research, 111,* B02408.

Ray, J., Altamimi, Z., Collilieux, X., & van Dam, T. (2007). Anomalous harmonics in the spectra of GPS position estimates. *GPS Solutions, 12*(1), 55–64.

Santamaría-Gómez, A. (2013). Very short baseline interferometry: assessment of the relative stability of the GPS stations at the Yebes Observatory (Spain). *Studia Geophysica et Geodaetica, 57*(2), 233–252.

Santamaría-Gómez, A., Bouin, M.-N., Collilieux, X., Wöppelmann, G. (2011). Correlated errors in GPS position time series: Implications for velocity estimates. *Journal of Geophysical Research, 116*(B1).

Schenewerk, M. S., Vandam, T. M., & Nerem, R. S. (1999). Seasonal motion in the Annapolis. *Maryland GPS monument. GPS Solutions, 2*(3), 41–49.

Schön, S. (2006). Affine distortion of small GPS networks with large height differences. *GPS Solutions, 11*(2), 107–117.

Stewart, M. P., Penna, N. T., & Lichti, D. D. (2005). Investigating the propagation mechanism of unmodelled systematic errors on coordinate time series estimated using least squares. *Journal of Geodesy, 79*(8), 479–489.

Tregoning, P., & van Dam, T. (2005). Atmospheric pressure loading corrections applied to GPS data at the observation level. *Geophysical Research Letters, 32*(22).

Wang, K., Chen, H., Jiang, W., Li, Z., Ma, Y., & Deng, L. (2018). Improved vertical displacements induced by a refined thermal expansion model and its quantitative analysis in GPS height time series. *Journal of Geophysics and Engineering, 15*(2), 554–567.

Wilkinson, M., Appleby, G., Sherwood, R., & Smith, V. (2013). Monitoring Site Stability at the Space Geodesy Facility. *Herstmonceux, UK, 138,* 95–102.

Williams, S. D. P. (2003). The effect of colored noise on the uncertainties of rates estimated from geodetic time series. *Journal of Geodesy, 76*(9–10), 483–494.

Williams, S. D. P. (2008). CATS: GPS coordinate time series analysis software. *GPS Solutions*, 147–153.

Williams, S. D. P., Bock, Y., Fang, P., Jamason, P., Nikolaidis, R. M., Prawirodirdjo, L., Miller, M., & Johnson, D. J. (2004). Error analysis of continuous GPS position time series. *Journal of Geophysical Research, 109*, B03412.

Wu, J. (2012). Propagation delay induced by antenna snow cover using PPP technology. *Geomatics & Information Science of Wuhan University, 37*(5), 617–620.

Xu, X., Dong, D., Fang, M., Zhou, Y., Wei, N., & Zhou, F. (2017). Contributions of thermoelastic deformation to seasonal variations in gps station position. *GPS Solutions, 21*(3), 1265–1274.

Yan, H., Chen, W., Zhu Y., Zhang, W., & Zhong, M. (2009). Contributions of thermal expansion of monuments and nearby bedrock to observed GPS height changes. *Geophysical Research Letters, 36*(13).

(Received November 25, 2017, revised March 12, 2018, accepted April 13, 2018, Published online April 23, 2018)